

---

# NEURAL POSTERIOR ESTIMATION FOR STOCHASTIC EPIDEMIC MODELING

---

A PREPRINT

**Prayag Chatha**  
Department of Statistics  
University of Michigan  
pchatha@umich.edu

**Fan Bu**  
Department of Biostatistics  
University of Michigan

**Jeffrey Regier**  
Department of Statistics  
University of Michigan

**Evan Snitkin**  
Department of Microbiology and Immunology  
University of Michigan

**Jon Zelner**  
Department of Epidemiology  
University of Michigan

## ABSTRACT

Stochastic infectious disease models capture uncertainty in public health outcomes and have become increasingly popular in epidemiological practice. However, calibrating these models to observed data is challenging with existing methods for parameter estimation. Stochastic epidemic models are nonlinear dynamical systems with potentially large latent state spaces, resulting in computationally intractable likelihood densities. We develop an approach to calibrating complex epidemiological models to high-dimensional data using Neural Posterior Estimation, a novel technique for simulation-based inference. In NPE, a neural conditional density estimator trained on simulated data learns to “invert” a stochastic simulator, returning a parametric approximation to the posterior distribution. We introduce a stochastic, discrete-time Susceptible Infected model with heterogeneous transmission for healthcare-associated infections (HAIs). HAIs are a major burden on healthcare systems, though they exhibit high rates of asymptomatic carriage, making it difficult to estimate infection rates. Through extensive simulation experiments, we show that NPE produces accurate posterior estimates of infection rates with greater sample efficiency compared to Approximate Bayesian Computation (ABC). We then use NPE to fit a SI model to an outbreak of carbapenem-resistant *Klebsiella pneumoniae*, a healthcare-associated infection (HAI), in a long-term acute care facility, finding evidence of location-based heterogeneity in patient-to-patient transmission risk. We argue that our methodology can be fruitfully applied to a wide range of mechanistic transmission models and problems in the epidemiology of infectious disease.

## 1 Introduction

Complex, mechanistic transmission models are a critical tool for the practice of infectious disease modeling and are increasingly used to make public health decisions in real time (Zelner and Eisenberg 2022). Epidemics are dynamical systems that feature an interplay of both deterministic forces and random events (Wood 2010; Hilborn and Mangel 2013), so stochastic models, which define a generative probability distribution of epidemics, have become prominent in epidemiology as computational resources have become more accessible (Daley and Gani 2001; Britton 2010). These models reflect the randomness of health outcomes in terms of both observational noise and the aleatoric nature of disease transmission through a population (He, Edward L Ionides, and A. A. King 2010), making them useful for informing public health policy under conditions of uncertainty.

The parameters governing stochastic epidemic models are often unknown and must be inferred from observational data. Bayesian inference offers a logical framework for estimating unobserved epidemiological parameters with uncertainty quantification and calibrating complex models to a given dataset (Dunson 2001). However, the difficulty of likelihood-based parameter estimation, the mainstay of classical statistical inference, has limited the design and viabil-

ity of stochastic epidemic models. Realistic transmission models are nonlinear dynamical systems with a potentially large state space of latent variables (e.g. corresponding to unobserved events such as recovery times) that result in intractable likelihood densities, thwarting conventional statistical tools (Bretó et al. 2009). In particular, individual-level models of infectious disease have likelihoods that may increase in exponential complexity with respect to the size of the population (Cauchemez and Ferguson 2011). In the Bayesian setting, recovering complete likelihoods involves computationally intensive sampling methods (e.g. data-augmented MCMC) that are tailored to a single model (Bu et al. 2022; Fintzi, Wakefield, and Minin 2022).

Forward sampling of data from stochastic dynamical systems is typically simpler and less expensive compared to evaluating their likelihood densities, motivating a class of methods for inference that treat models as black-box simulators. Prominent examples of these include Iterated Filtering (Edward L Ionides, Bretó, and A. A. King 2006; Edward L. Ionides et al. 2011) and Approximate Bayesian Computation (ABC, M. A. Beaumont 2010; Toni and Stumpf 2010). Iterated Filtering makes the assumption that observations and latent variables are jointly Gaussian (a problematic assumption in small-population settings) and can be prohibitively slow when used for Bayesian inference. ABC has been applied to epidemiology (McKinley et al. 2018; Minter and Retkute 2019), but as a Monte Carlo sampling method it suffers from the curse of dimensionality, making it prohibitively expensive in many settings and reliant on low-dimensional summary statistics designed by domain experts (Cranmer, Brehmer, and Louppe 2020; Lueckmann, Boelts, et al. 2021).

Neural Posterior Estimation (NPE) is a novel technique for approximate Bayesian inference, in which a neural network trained on simulated data learns predicts likely model parameters, effectively learning how to “invert” a forward simulation model with an intractable likelihood (Papamakarios and Murray 2016). NPE can be understood as automatically learning important features (i.e. summary statistics) from raw data in order perform approximate posterior inference. NPE is simple to adapt to a given simulator. Once trained, NPE can draw posterior samples—conditioning on any dataset—cheaply and in parallel, in contrast to Monte Carlo methods. NPE belongs to an emerging family of simulation-based, deep learning-powered inference methods (e.g. Papamakarios 2019) that scale efficiently to high-dimensional data (Cranmer, Brehmer, and Louppe 2020). These algorithms have been used for statistical inference in a wide range of scientific domains, including including neuroscience (Lueckmann, Goncalves, et al. 2017), particle physics (Baydin et al. 2019), and astronomy (R. Liu et al. 2023; Dax et al. 2021; Vasist et al. 2023).

In this article, we develop an approach to calibrating realistic epidemic models with NPE. While NPE has been previously used to estimate the parameters of deterministic compartmental models in ecology and epidemiology (notably, Radev et al. 2021), to our knowledge this is the first work to apply deep learning and simulation-based inference to fully stochastic epidemic models, which are distinctly challenging for classical model-fitting techniques such as ordinary least squares. While our approach is compatible with a wide variety of epidemiological models, we focus our attention on the problem of inferring heterogeneous transmission patterns in healthcare-associated infections (HAIs). HAIs are among the top 10 causes of death in the US and are associated with billions of dollars of excess healthcare costs (Healthcare Research and Quality 2024), making them a significant public health issue. Compared to other environments, hospitals offer researchers detailed data on individual mobility (which tends to be limited) and infection times; they are a natural setting for prototyping stochastic epidemic models with spatially-dependent transmission. Accurate modeling of HAI transmission has the potential to inform mitigation policies within the healthcare system.

The rest of this article is organized as follows: in Section 2, we provide an overview of the NPE algorithm for Bayesian simulation based inference. In Section 3, we present a heterogeneous stochastic susceptible-infected (SI) model for interpreting healthcare-associated infections. Through extensive simulation experiments, we demonstrate that NPE can be used to efficiently produce accurate posterior approximations of infectious disease parameters. In Section 4, we use NPE and stochastic SI models to analyze a real-world dataset, an intervention carried out against carbapenem-resistant *Klebsiella pneumoniae* (CRKP) at a Chicago-area long-term acute care hospital (LTACH) over the course of a year. We discuss our results and make recommendations for a simulation-based inference workflow in Section 5 before pointing to future research directions in Section 6.

## 2 Simulation-Based Inference

Let  $\mathbf{x} = x_1, \dots, x_N$  denote a data sample of  $N$  exchangeable observations, and let  $\theta$  be an unobserved parameter of interest. We assume that the data depend on  $\theta$  through a likelihood  $p(\mathbf{x} | \theta)$  and that  $\theta$  follows a prior distribution  $p(\theta)$ . We seek to compute the posterior distribution of  $\theta$  conditioned on some observed dataset  $\mathbf{x}_o$ ,

$$p(\theta | \mathbf{x}_o) = \frac{p(\theta)p(\mathbf{x}_o | \theta)}{p(\mathbf{x}_o)}. \quad (1)$$

Now suppose, under our data generating model, that the likelihood is a *simulator* with an intractable density function from which we nevertheless can sample simulated data. A prototypical simulator is a computer program that takes

parameters  $\theta$  as inputs, samples a sequence of random internal states (that is, latent variables)  $\mathbf{z}_t \sim p(\mathbf{z}_t \mid \theta, \mathbf{z}_{<t})$ , and finally, as output, generates data  $\mathbf{x} \sim p(\mathbf{x} \mid \theta, \mathbf{x})$ . If the latent space, typically corresponding to the stochastic evolution of a dynamical system, is large enough, the data likelihood

$$p(\mathbf{x} \mid \theta) = \int p(\mathbf{x}, \mathbf{z} \mid \theta) d\mathbf{z} \quad (2)$$

will be a high-dimensional integral, making likelihood-based posterior inference prohibitively costly.

Approximate Bayesian Computation (ABC) is a popular and well-established approach to Bayesian simulation-based inference (SBI) (Sisson, Fan, and M. Beaumont 2018). In ABC, we compare a large number of simulated datasets to the observed data based on user-specified summary statistic(s)  $g(\cdot)$ , accepting parameters for simulations that fall within an  $\epsilon$ -ball of  $g(\mathbf{x}_o)$ . (See Appendix B for a sketch of the basic ABC algorithm.) This results in a nonparametric, Monte Carlo sample whose limiting distribution is  $p(\theta \mid \|g(\mathbf{x}) - g(\mathbf{x}_o)\| < \epsilon)$ , an approximation of  $p(\theta \mid g(\mathbf{x}_o))$ . As  $\epsilon$  is decreased, the posterior approximation gets more accurate yet samples are more likely to be rejected, increasing the computational cost. To achieve a modest reduction in  $\epsilon$  it may be necessary to run orders of magnitude more simulations; tuning  $\epsilon$  to strike a balance between accuracy and speed may be difficult.

As a Monte Carlo sampling method, the number of samples required to explore the parameter space and find simulations that are similar to observed data increases exponentially in the dimension of  $\theta$  and  $g(\mathbf{x})$ : the so-called curse of dimensionality. Summary statistics are a possible means of improving computational efficiency, but they will generally incur a loss of posterior information, making all inference approximate.<sup>1</sup> Domain expertise may inform the choice of summary statistics, but the best choice is not always clear, in which case statistics may be engineered ad hoc. To improve the efficiency of ABC, it is often suggested that parameters be sampled from a *proposal distribution*  $\tilde{p}(\theta)$  which is (somehow) known to be close to the posterior. In practice, this is a circular logic: a good proposal distribution that leverages your belief about the posterior is essentially a better prior by another name.

Like ABC, NPE approximates the posterior distribution without direct evaluation of the likelihood density. Unlike ABC, NPE achieves this by optimizing a *neural conditional density estimator*  $q_\phi(\cdot \mid \cdot)$  to learn the density of  $\theta$  conditional on  $\mathbf{x}$  for *arbitrary*  $\theta$  and  $\mathbf{x}$  sampled from the model joint distribution the joint generative model  $p(\theta, \mathbf{x}) = p(\theta)p(\mathbf{x} \mid \theta)$ . The encoder network is more likely to learn an accurate approximation of a specific posterior if it has encountered many samples from the joint distribution during training. By learning the general posterior, NPE is performing *amortized inference*. We constrain  $q_\phi$  to belong to a parametric family of densities;  $\phi$  defines a neural network encoder that outputs the parameters of the conditional density. We train the encoder to learn the general posterior by maximizing the objective function

$$\mathbf{E}_{p(\theta, \mathbf{x})}[\log q_\phi(\theta \mid \mathbf{x})] \quad (3)$$

with respect to  $\phi$ , using Stochastic Gradient Descent or a variant thereof. We outline NPE in Algorithm 1. Once the encoder network is trained, we can easily produce a posterior distribution conditional on any dataset, providing fast Bayesian inference for new observations.

---

#### Algorithm 1 Amortized Neural Posterior Estimation

---

**Input:** Prior distribution  $p(\theta)$ , simulator  $p(\mathbf{x} \mid \theta)$ , neural conditional density estimator  $q_\phi(\cdot \mid \cdot)$ , observed data  $\mathbf{x}_o$

**Output:** Approximate posterior distribution  $\hat{p}(\theta \mid \mathbf{x}_o)$

**for**  $s = 1, 2, \dots, S$  **do**

Sample  $\theta_s \sim p(\theta)$

Simulate  $\mathbf{x}_s \sim p(\mathbf{x} \mid \theta_s)$

**end for**

Using stochastic gradient descent, solve

$$\phi^* = \arg \min_{\phi} -\frac{1}{S} \sum_{s=1}^S \log q_\phi(\theta_s \mid \mathbf{x}_s) \quad (4)$$

$\hat{p}(\theta \mid \mathbf{x}_o) \leftarrow q_{\phi^*}(\theta \mid \mathbf{x} = \mathbf{x}_o)$

---

NPE turns the problem of sampling from the posterior into an optimization problem, making it analogous to standard Variational Inference (VI), where the evidence lower bound (ELBO) loss function depends on the likelihood density.

<sup>1</sup>Outside of the exponential family, it is difficult, if not impossible, to find *sufficient* summary statistics of finite dimension (cf. the Pitman-Koopman-Darmois theorem).

Ambrogioni et al. (2019) showed that maximizing Equation 3 is equivalent to minimizing the forward KL-Divergence between the model distribution  $p(\boldsymbol{\theta}, \mathbf{x})$  and the *joint variational distribution*  $q(\boldsymbol{\theta}, \mathbf{x}) = q_\phi(\boldsymbol{\theta} | \mathbf{x})k(\mathbf{x})$ , where  $k(\mathbf{x})$  is the sampling distribution of the simulated training data used to fit  $q_\phi$ . Alternatively, we can think of NPE as nonlinear, heteroscedastic regression of parameters  $\boldsymbol{\theta}$  on simulated data  $\mathbf{x}$  in order to obtain a conditional probability distribution (Blum and François 2010). Once the conditional density estimator is trained, sampling from the posterior is a simple, parallelizable operation, in contrast to Monte Carlo samplers. Furthermore, it is trivial to obtain the posterior conditioned on a new dataset, though NPE requires training a new network if the model is changed.

One of the virtues of NPE is its simplicity: sampling from the approximate posterior requires training a single neural network and obtaining its prediction for a given dataset. NPE was introduced alongside “sequential” variations that involve learning better proposal distributions for  $\boldsymbol{\theta}$  from the data (Papamakarios and Murray 2016; Lueckmann, Goncalves, et al. 2017), pursuing greater sample efficiency in exchange for multiple training cycles. We argue that the one-stage NPE procedure is less brittle, more user-friendly, and still offers considerable efficiency gains. Alternative techniques for simulation-based inference also use neural networks to learn a conditional density, such as Neural Likelihood Estimation (NLE, Papamakarios 2019), though these methods that avoid estimating the posterior directly have to be paired with a sampling scheme (i.e. MCMC).

After a data generative model has been selected, NPE entails two principal design choices: (1) the form of the conditional density estimator and (2) the encoder’s neural network architecture. First, to achieve a decent approximation of the target posterior, the conditional density estimator  $q_\phi$  must define a sufficiently expressive “variational family” of distributions. Gaussian Mixture Models (Papamakarios and Murray 2016), Normalizing Flows (Papamakarios, Nalisnick, et al. 2021), and Diffusion Models (Simons et al. 2023) have been proposed as conditional density estimators due to their ability to model complex, multimodal posterior distributions. However, these algorithms may be more complicated than necessary, since many posterior distributions arising in scientific problems are unimodal and relatively narrow—that is, approximately Gaussian. The practice of approximating an unknown posterior using a Gaussian dates back to Laplace, and this method has some theoretical justification (see Section 5). In our experiments, we use transformed univariate and multivariate Gaussian distributions as our approximation family, as easy to optimize and often sufficiently precise. Hence, we take  $q_\phi(\boldsymbol{\theta} | \mathbf{x}) = \mathcal{N}(\boldsymbol{\theta} | \boldsymbol{\mu}(\mathbf{x}), \boldsymbol{\Sigma}(\mathbf{x}))$ , where the mean vector  $\boldsymbol{\mu}$  and covariance matrix  $\boldsymbol{\Sigma}$  are functions of the data that a neural network learns.

Second, the encoder network must have an architecture capable of learning the posterior from simulations. In a sense, the role of the encoder network is analogous to the use of handcrafted summary statistics in ABC, except that a neural network can automatically learn compact feature representations from high-dimensional, possibly hierarchical data. We note that standard neural networks are not invariant to permutations of data. Therefore, to satisfy the assumption of exchangeable observations, it is necessary to *pool* the data e.g. sum key descriptives over the sample indices. In this respect, NPE requires some minimal summarization of the data, though pooled time series data can still be quite high dimensional. We employ a three-layer feedforward neural network as our encoder architecture, with the network width and weight decay regularization (Loshchilov, Hutter, et al. 2017) as our hyperparameters. In all experiments, we use a 75-25 training/validation split of simulations along with early stopping to ensure that the encoder generalizes well to unseen data.

### 3 A Susceptible-Infected Model of Healthcare-Associated Infection

In this section, we develop a discrete-time, stochastic compartmental model with heterogeneous infection rates for modeling healthcare-associated infections. A prototypical HAI is a bacteria that colonizes patients through the vector of healthcare workers. Asymptomatic colonization may be widespread, but some colonizations may erupt into life-threatening invasive infections (e.g. by entering the bloodstream through an indwelling medical device).

We propose a Susceptible-Infected (SI) model<sup>2</sup> for HAIs, since colonized patients tend to remain colonized, barring medical intervention. A “recovered” state for individuals is inappropriate since recolonization may occur at any point. Hospitals and other care facilities are generally small-population settings, which means that aggregate disease spread appears non-deterministic. Subjects are also monitored relatively frequently and regularly. For these reasons, a discrete-time stochastic model is appropriate for describing HAI transmission.

We develop this stochastic transmission model and its variants from basic epidemiological principles and show that it is possible to interpret this model both as an analytic likelihood and as a simulation program. In the case of partial observation of cases, the corresponding likelihood density is computationally intractable, but the data simulator is not. Through extensive simulation experiments, we show that simulation-based inference is an effective methodology

<sup>2</sup>A “Colonized-Uncolonized model” would be more precise in this case, but we match the terminology more widely used in epidemic modeling.

for estimating key parameters and fitting an abstract transmission model to noisy data. We also show that in many instances, NPE is a more efficient and robust parameter estimation procedure than Approximate Bayesian Computation (ABC), the established mode of Bayesian simulation-based inference.

### 3.1 SI Model with Heterogeneous Infection Rates

Suppose we observe a healthcare facility with a population of  $N$  patients over  $T$  time steps. For each individual  $i = 1, \dots, N$ , let the binary variable  $X_t^{(i)}$  represent their disease status at discrete time intervals  $t = 1, \dots, T$ . If a patient is infected by time  $t$ , then  $X_t^{(i)} = 1$ , otherwise  $X_t^{(i)} = 0$ . Let  $S_t$  and  $I_t$  denote the number of susceptible and infected patients in the facility at time  $t$ . Patients are either susceptible or infected, so  $S_t + I_t = N$  for all  $t$ .

We model the transitions of individuals from the susceptible compartment to infected compartment as stochastically. Let  $\lambda_i(t)$  denote the *force of infection* acting on a susceptible individual  $i$  at time step  $t$ . We can think of the force of infection as an individualized hazard function. We assume  $\lambda_i$  is constant over each discrete interval  $[t, t - 1)$  and that each individual infection event is an exponentially-distributed event with rate parameter  $\lambda_i(t)$ . Over small enough time steps, this is a reasonable assumption (A. King 2024). Then,

$$P(X_t^{(i)} | X_{t-1}^{(i)} = 0) = (1 - e^{-\lambda_i(t)})^{X_t^{(i)}} (e^{-\lambda_i(t)})^{1-X_t^{(i)}} \quad (5)$$

This formulation results in binomial sampling of cases (i.e. a binomial chain model). Each individual's trajectory  $\mathbf{X}^{(i)} = \{X_1^{(i)}, \dots, X_T^{(i)}\}$  is a stochastic process, namely, a discrete-time, non-homogeneous Markov Chain.

#### 3.1.1 Individualized Force of Infection

Stochastic epidemic models, unlike their deterministic analogs, have the capacity to model transmission events at the individual level. We allow the force of infection to vary based on the location of the susceptible individual and infectious patients. Suppose that the facility comprises  $K$  floors and  $R$  rooms. We consider a vector of heterogeneous infection rates,  $\beta = (\beta_0, \beta_1, \dots, \beta_{K+1})$ , where each  $\beta_j > 0$ . These rates signify the following:

- $\beta_0$  is the *facility rate*, the transmission rate between any infected-susceptible pair of patients in the facility;
- $\beta_k$  is the *floor rate*, the rate of infection between an infected and susceptible patient who both reside on floor  $k$  for  $k = 1, \dots, K$ ;
- $\beta_{K+1}$  is the *room rate*, the transmission rate between a susceptible and infected patient who share a room. This effect is fixed across all rooms.

Let  $F(i) \in \{1, \dots, K\}$  denote the floor where patient  $i$  is staying at timestep  $t$ . The contribution of an infected patient  $j$  to the force of infection acting on an infected patient  $i$  is

$$\lambda_{i \leftarrow j} = \begin{cases} \frac{\beta_0}{N} + \frac{\beta_{F(i)}}{N_F} + \frac{\beta_{K+1}}{N_R} & \text{if } i \text{ and } j \text{ are roommates,} \\ \frac{\beta_0}{N} + \frac{\beta_{F(i)}}{N_F} & \text{if } i \text{ and } j \text{ are floormates,} \\ \frac{\beta_0}{N} & \text{otherwise.} \end{cases} \quad (6)$$

Then, the aggregate force of infection acting on an individual is

$$\lambda_i(t) = \sum_{j: X_{t-1}^{(j)}=1} \lambda_{i \leftarrow j}. \quad (7)$$

The force of infection is a linear expression depending on the proximity of infectious patients to a susceptible target patient. Since all  $\beta_j$  are positive, we tacitly assume that the infection risk increases with proximity, e.g. the force of infection between roommates is greater than that between floormates who don't share a room.

With some notational effort, we can write out a compact expression for the total individualized force of infection for any patient. Let  $C_F$  and  $C_R$  denote the size  $N \times N$  floor-level and room-level contact matrices.<sup>3</sup> If patients  $i$  and  $j$

<sup>3</sup>If patients' locations are allowed to change over the course of their stay, then these matrices need to be recomputed every time step. For readability's sake we suppress the time dependency in notation.

reside on the same floor, then entry  $C_F[i, j]$  is 1 and 0 otherwise.  $C_R$  is constructed similarly. For any  $t$ , we treat  $X_t$  as a  $N \times 1$  column vector. If patient  $i$  is infected at time  $t$ , then the  $i$ -th entry  $X_t[i]$  is 1 and 0 otherwise.<sup>4</sup> Then,

$$\lambda_i(t) = (\beta_0 \cdot \mathbf{1}^\top X_{t-1} + \beta_{F(i)} \cdot C_F[i]^\top X_{t-1} + \beta_{K+1} \cdot C_R[i]^\top X_{t-1}), \quad (8)$$

Homogeneous transmission (i.e. random mixing) is a special case of this heterogeneous model. Supposing we ignore patient location, then the force of infection depends only on the facility-level infection rate,  $\beta = \beta_0$ . Therefore,

$$\lambda_i(t) = \sum_{j: X_{t-1}^{(j)}=1} \beta = \beta \frac{I_{t-1}}{N}. \quad (9)$$

### 3.1.2 Random Intake and Outtake

Healthcare facilities see rapid turnover of patients on the timescales of disease transmission. Often, patients are pre-colonized when they enter the facility, increasing the overall risk of infection. Conversely, colonized patients may be discharged, reducing the disease's effective reproductive rate. Random turnover also increases the noise of the epidemic process. Patient intake and outtake affects the dynamics of transmission, so it is important for a model to take these movements and outside colonization into account.

In a real-world study, we can expect to have data on patient admission and discharge times and whether they screened for infectious disease(s) upon intake. We can treat these as non-random events in a transmission model (see Section 4). For the purpose of simulation experiments, we suppose that, at any time step, patients are discharged with a fixed probability and immediately replaced (i.e. facility stays at full capacity). We also suppose that patients enter the facility with a fixed probability of carrying the infection in question. This disease model can be likened to a stochastic counterpart to the (deterministic) Ross-Macdonald model (Ross 1911; Macdonald, G 1957), a classical model for the transmission of mosquito-borne malaria. Here, mobile healthcare workers act as the disease vector between stationary patients (Doan et al. 2014).

With turnover of patients, the sample index  $i = 1, \dots, N$  now technically refers to individual *locations* (e.g. patient beds) that host multiple as they move in and out of the facility and possibly between locations during their stay. Let  $\gamma$  denote the probability of a patient being discharged (and immediately replaced) in between time steps  $t$  and  $t + 1$ , and let  $\alpha$  measure the population proportion of already-colonized individuals entering the facility. (We also sample the initial infections from a binomial draw with probability  $\alpha$ .) We assume that  $\alpha$  and  $\gamma$  are both known parameters, unlike the infection rates.

To recapitulate, the status  $X_t^{(i)}$  of the patient at location  $i$  and time  $t$  may change due to one of three random events. We list these transition events along with their probabilities:

1.  $P(\text{a patient is replaced by an infected}) = \gamma\alpha$
2.  $P(\text{a patient is replaced by a susceptible}) = \gamma(1 - \alpha)$
3.  $P(\text{a susceptible patient } i \text{ becomes infected}) = (1 - \gamma) \cdot (1 - e^{-\lambda_i(t)})$

We assume that a susceptible patient cannot get infected until the time step after they are admitted. Therefore, a freshly admitted patient is immune from infection, explaining the  $(1 - \gamma)$  term in events 3. We outline the complete data generating process as a simulation program in Algorithm 2.

With random turnover of patients, infectious patients are eventually removed from the system, so the basic reproduction number  $\mathcal{R}_0$  is defined.<sup>5</sup> Calculating  $\mathcal{R}_0$  is straightforward when the infection rate is homogeneous. Patient stay lengths are geometrically distributed, so the average stay length of an infectious patient (before they are replaced by a susceptible patient) is  $1/(\gamma(1 - \alpha))$ . Therefore,

$$\mathcal{R}_0 = \frac{\beta}{\gamma(1 - \alpha)}. \quad (10)$$

In the case of a heterogeneous model,

$$\mathcal{R}_0 = \frac{\bar{\beta}}{\gamma(1 - \alpha)} \quad (11)$$

<sup>4</sup>That is,  $X_t[i] \equiv X_t^{(i)}$ .

<sup>5</sup>That is, the average period of infectiousness is finite. Without turnover, this average period of infectiousness is effectively  $T$ , the full period of observation.

**Algorithm 2** Stochastic Discrete-time SI Simulator

**Input:** Vector of transmission rates  $\beta$ , discharge probability  $\gamma$ , population proportion of infected  $\alpha$ , floor assignments  $\mathbf{k}$ , room assignments  $\mathbf{r}$

**Output:**  $N \times T$  matrix  $\mathbf{X}$  of infection logs  $\mathbf{X}^{(i)} = \{X_1^{(i)} \dots X_T^{(i)}\}$  for all patients  $i = 1, \dots, N$

Initialize infecteds as  $X_1^{(i)} \sim \text{Bernoulli}(\alpha)$

**for**  $t = 2, \dots, T$  **do**

**for**  $i \in 1, \dots, N$  **do**

    Draw  $D_t^{(i)} \sim \text{Bernoulli}(\gamma)$

**if**  $D_t^{(i)} = 1$  **then**

$\triangleright$  patient  $i$  is discharged and replaced

      Draw  $X_t^{(i)} \sim \text{Bernoulli}(\alpha)$

**else**

**if**  $X_{t-1}^{(i)} = 0$  **then**

$\triangleright$  patient  $i$  is susceptible

        Compute the individualized force of infection  $\lambda_i(t)$

        Draw  $X_t^{(i)} \sim \text{Bernoulli}(1 - e^{-\lambda_i(t)})$

**else**

$X_t^{(i)} \leftarrow 1$

**end if**

**end if**

**end for**

**end for**

where

$$\bar{\beta} = \beta_0 + \frac{1}{K} \sum_{j=1}^K \beta_j + \beta_{K+1}. \quad (12)$$

We need to average out the within-floor infection rates, since an infected individual may reside in only one floor.

**3.1.3 Model Likelihood**

Given an observed dataset  $\mathbf{X}$  of patient statuses over time, we can write out the likelihood of a vector of infection rates  $\beta$ . Let  $X_t = (X_t^{(1)}, \dots, X_t^{(N)})$ , the array of patient statuses at time  $t$ . At the start of the observation period ( $t = 1$ ), we sample initial statuses from a Bernoulli with probability  $\alpha$ , the external proportion of infection. Then,

$$P(X_1) = \prod_{i=1}^N \alpha^{X_1^{(i)}} (1 - \alpha)^{1 - X_1^{(i)}} \quad (13)$$

For subsequent time steps  $t = 2, \dots, T$ , we can write an autoregressive conditional probability as

$$P(X_t | X_{t-1}) = \prod_{i=1}^N \left( [\gamma\alpha + (1 - \gamma)]^{X_{t-1}^{(i)}} \cdot [\gamma\alpha + (1 - \gamma)(1 - e^{-\lambda_i(t)})]^{(1 - X_{t-1}^{(i)})} \right)^{X_t^{(i)}} \cdot \left( [\gamma(1 - \alpha)]^{X_{t-1}^{(i)}} \cdot [\gamma(1 - \alpha) + (1 - \gamma)(e^{-\lambda_i(t)})]^{(1 - X_{t-1}^{(i)})} \right)^{(1 - X_t^{(i)})}. \quad (14)$$

Let  $\mathbf{X} = X_1, \dots, X_T$ . The complete likelihood over all time steps then factorizes as

$$p(\mathbf{X} | \beta) = P(X_1) \cdot \prod_{t=2}^T P(X_t | X_{t-1}). \quad (15)$$

See Section B.3 for a derivation of the likelihood. The likelihood has a complexity of  $O(T \cdot N^2)$ . At every time step, the probability of a patient getting infected depends non-trivially on the status of all other patients in the facility via the force of infection  $\lambda_i(t)$  (Equation 8). In the simpler case of a homogeneous infection rate, the likelihood complexity is  $O(T \cdot N)$ .

**3.1.4 Partial Observation of Cases**

A patient colonized with a nosocomial disease will often show no symptoms unless the infection becomes invasive (e.g., bacteria move from the surface of the skin to internal organs). For this reason, it is unrealistic to assume that

all patient infection statuses will be observed, barring extensive prospective surveillance of individuals: a majority of infected patients may be asymptomatic carriers. To address this problem, we extend the stochastic SI model to the scenario of *partial observation*.

We introduce a new status variable  $Y_t^{(i)}$ , that indicates whether the patient at location  $i$  is observably infected by time step  $t$ . Analogously to  $X_t^{(i)}$ , let  $Y_t = (Y_t^{(1)}, \dots, Y_t^{(N)})$  and let  $\mathbf{Y} = Y_1, \dots, Y_T$ :  $\mathbf{Y}$  denotes our observed data, the observed cases over time. In this variant of the SI model, the old status variable  $X_t^{(i)}$  reflects asymptomatic infection (colonization) with the pathogen of interest. We observe a colonized patient’s infection either because they are experiencing invasive symptoms or because they were screened for pathogens upon entry. We extend our data generating process to  $Y$  on the basis of four simple rules.

1. If a location  $i$  admits a new patient at time step  $t$ , they are tested upon admission, then we observe their status. Therefore,  $Y_t^{(i)} = X_t^{(i)}$
2. At any time step  $t$ , a colonized but hitherto asymptomatic patient will show symptoms with probability  $\eta \in (0, 1]$ . That is,  $Y_t^{(i)} \sim \text{Bernoulli}(\eta)$ .
3. An uncolonized patient will never show symptoms:  $X_t^{(i)} = 0 \implies Y_t^{(i)} = 0$
4. A symptomatic patient will remain symptomatic. Assuming there is no turnover at location  $i$  during time step  $t$ ,  $Y_{t-1}^{(i)} = 1 \implies Y_t^{(i)} = 1$ .

$\eta$  is the *probability of observation*, which we can interpret as the chance of an asymptomatic infection going invasive during any one time step. While we might have reason to believe that the probability of observation depends on individual-level covariates (e.g. age, comorbidities) and/or time spent in the facility, for simplicity’s sake we assume a homogeneous and constant  $\eta$ . In this model, the time it takes for a colonized patient to show symptoms follows a geometric distribution, which can be thought of as a discretized exponential distribution. The formula for the force of infection is the same as for the fully observed heterogeneous SI model (Equation 8).

In Algorithm 3, we describe the simulator corresponding to the forward data generating model under partial observation of cases. With some effort, we could write out the *complete likelihood*,  $p(\mathbf{Y}, \mathbf{X} | \beta) = p(\mathbf{Y} | \mathbf{X})p(\mathbf{X} | \beta)$ , using the the aforementioned rules to compute the conditional probability of observed infection  $p(\mathbf{Y} | \mathbf{X})$ . (In Appendix D, we sketch a derivation of  $p(\mathbf{Y} | \mathbf{X})$  in the simplest case of no random turnover, i.e.  $\gamma = 0$ .) Generally, computing the observed data likelihood  $p(\mathbf{Y} | \beta)$  is infeasible, as it entails integrating the complete likelihood over all possible configurations of  $\mathbf{X}$ , a massive state space when the force of infection is heterogeneous. Heuristically speaking,

$$p(\mathbf{Y} | \beta) \approx \sum_{\mathbf{X}} p(\mathbf{Y}, \mathbf{X} | \beta). \quad (16)$$

Critically,  $\mathbf{X}$  has  $2^{T \cdot N}$  configurations, though not all of these are permissible given a set of observed infection times  $\mathbf{Y}$ . Therefore, the observed data likelihood has a (worst-case) complexity of  $O(2^{T \cdot N} T \cdot N^2)$ . When the force of infection is heterogeneous, marginalizing over many unobserved  $X_i$  is computationally intensive.

### 3.2 Experiment I: Homogeneous Transmission

For our first simulation consider the problem of inferring an unknown, homogeneous infection rate  $\beta$ . We fix this rate’s true value to be  $\beta^* = 0.15$  and suppose a lognormal<sup>6</sup> prior,  $\beta \sim \text{Lognormal}(-3, 1)$ , or equivalently,  $\log(\beta) \sim \mathcal{N}(-3, 1)$ . We set the remaining simulation parameters to be  $N = 100$ ,  $T = 52$ ,  $\alpha = 0.1$ , and  $\gamma = 0.05$ , resulting in true  $\mathcal{R}_0$  of 10/3. We take a single simulation from the resulting SI model to be our “observed” data,  $\mathbf{X}_o$ . In Figure 1a, we visualize  $\mathbf{X}_o$  by showing the proportion of infected and susceptible patients over time. Observe that by time step 40, the proportion infected appears to plateau at around 0.7, the herd immunity threshold determined by  $\mathcal{R}_0$ .

As a benchmark for our simulation-based approximations of the posterior, we compute a likelihood-based estimate of the exact posterior  $p(\beta | \mathbf{X}_o)$  using Rejection Sampling, a likelihood-based analog to ABC (Appendix B). We generated a posterior sample of size 100, which required just under 2,000 independent draws from the prior. We estimated that the exact posterior  $p(\beta | \mathbf{X}_o)$  has a mean of 0.137, close to the true value of  $\beta$ . On the log scale, the posterior sample appears approximately normal, with a mean of -1.99 and a standard deviation of 0.0949.

We use NPE to learn a lognormal approximation to the posterior of  $\beta$  from simulated realizations of the stochastic SI model. We pool the observed data by summing over the patient index  $i$ , taking as our input data the total count of

<sup>6</sup>The lognormal, along with the gamma distribution, is commonly used for parametrically modeling a positive random variable such as a rate parameter. Even in multiple dimensions, sampling from a lognormal prior is trivial.

**Algorithm 3** Stochastic SI Simulator with Partial Observation

---

**Input:** Vector of transmission rates  $\beta$ , discharge probability  $\gamma$ , population proportion of infected  $\alpha$ , floor assignments  $\mathbf{k}$ , room assignments  $\mathbf{r}$ , probability of observation  $\eta$

**Output:**  $N \times T$  matrix  $\mathbf{Y}$  of observed case logs  $\mathbf{Y}^{(i)} = \{Y_1^{(i)} \dots Y_T^{(i)}\}$  for all patients  $i = 1, \dots, N$

Initialize array of colonization statuses  $X_1^{(i)} \sim \text{Bernoulli}(\alpha)$

Set  $Y_1^{(i)} \leftarrow X_1^{(i)}$

**for**  $t = 2, \dots, T$  **do**

**for**  $i \in 1, \dots, N$  **do**

    Draw  $D_t^{(i)} \sim \text{Bernoulli}(\gamma)$

**if**  $D_t^{(i)} = 1$  **then** ▷ patient  $i$  is discharged and replaced

      Draw  $X_t^{(i)} \sim \text{Bernoulli}(\alpha)$

**else**

**if**  $X_{t-1}^{(i)} = 0$  **then** ▷ patient  $i$  is susceptible

        Compute the individualized force of infection  $\lambda_i(t)$

        Draw  $X_t^{(i)} \sim \text{Bernoulli}(1 - e^{-\lambda_i(t)})$

**else**

$X_t^{(i)} \leftarrow 1$

**end if**

**end if**

**if**  $D_t^{(i)} = 1$  **then** ▷ screen newly admitted patient  $i$

$Y_t^{(i)} \leftarrow X_t^{(i)}$

**else if**  $X_t^{(i)} = 1 \wedge Y_{t-1}^{(i)} = 0$  **then**

      Draw  $Y_t^{(i)} \sim \text{Bernoulli}(\eta)$

**else**

$Y_t^{(i)} \leftarrow Y_{t-1}^{(i)}$

**end if**

**end for**

**end for**

---

infecteds over time,  $\mathbf{I} = \{I_1, \dots, I_T\}$ .  $\mathbf{I}$  is a time series vector of length 52 and a minimal summary of the raw data  $\mathbf{X}$ . We stress that  $\mathbf{I}$  is not a sufficient statistic for  $\beta$  in the strict sense, at least when  $\gamma > 0$ , however, we find empirically that we can fit highly accurate posterior estimates of  $\beta$  using just  $\mathbf{I}$ . Our approximate posterior inference procedure assumes that

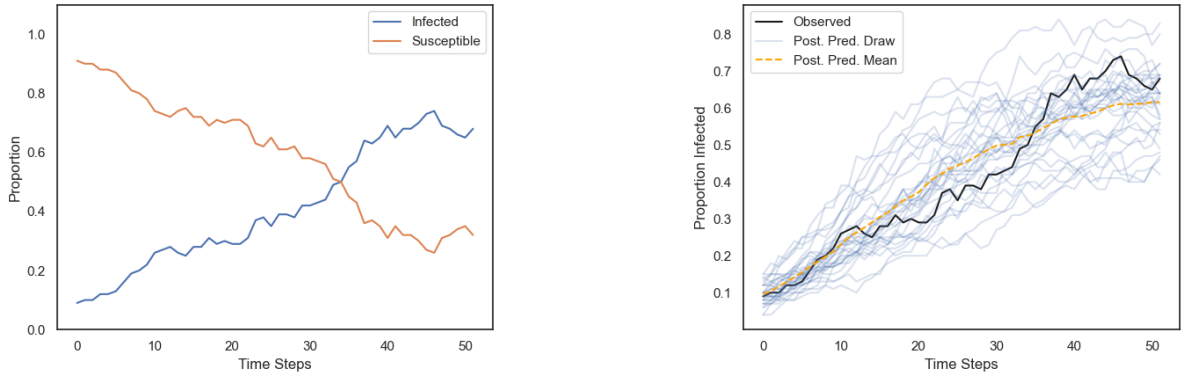
$$\hat{p}(\log(\beta) \mid \mathbf{I}) \approx p(\log(\beta) \mid \mathbf{I}) \approx p(\log(\beta) \mid \mathbf{X}), \quad (17)$$

where  $\hat{p}$  denotes a simulation-based estimate of  $p$ .

Trained on 4,000 simulations from the forward model, NPE converged on the approximation  $\hat{p}(\beta \mid \mathbf{I}_o) = \text{Lognormal}(\mu = -1.99, \sigma = 0.15)$ , resulting in a posterior mean estimate of  $\hat{\beta} = 0.139$ . The NPE posterior approximation is virtually unbiased (see Figure 2) with respect to the exact posterior and only slightly more dispersed. We hypothesize that this variance gap is explained by the loss of information from working with  $\mathbf{I}$  instead of  $\mathbf{X}$ . In Figure 1b, we illustrate the posterior predictive distribution of  $p(\mathbf{I} \mid \mathbf{I}_o)$  resulting from our NPE approximation of  $p(\beta \mid \mathbf{I}_o)$ . The posterior predictive mean, estimated from 30 posterior draws of  $\beta$ , smoothly interpolates the curve depicting the proportion of infected patients over time.

In Figure 3, we illustrate the accuracy and sample efficiency trade-off of ABC and NPE in terms of the estimated posterior mean (Figure 3a) and variance (Figure 3b). We evaluate two versions of ABC, one that matches the total case-count time series  $\mathbf{I}$  and another, denoted as ABC-S, that matches a scalar summary of the data,  $g(\mathbf{I}) = T^{-1} \sum_{t=1}^T I_t$ , i.e. the average of the time series  $\mathbf{I}$ . For both ABC and ABC-S, we drew parameters from the prior until 100 were accepted.<sup>7</sup> Interestingly, we find that this choice of summary statistic does not significantly help (or hinder) the performance of ABC. The posterior mean accuracy of ABC-S is slightly worse, implying that the summary statistic incurs minimal information loss, yet it demonstrates no improvements in efficiency. One explanation is that  $\mathbf{I}$ , despite

<sup>7</sup>The efficiency of ABC obviously depends on the desired size of the posterior sample. We took 100 to be a sufficiently large size such that sampling error is reasonably small. In practice, a statistician may generate a Monte Carlo sample of size 1,000 or more.



(a) Realization of a stochastic SI model with homogeneous transmission serving as the observed data.

(b) Posterior predictive check of the NPE estimate of the rate of infection  $\beta$

Figure 1: NPE Calibration of a stochastic SI model with a homogeneous infection rate to a simulated epidemic

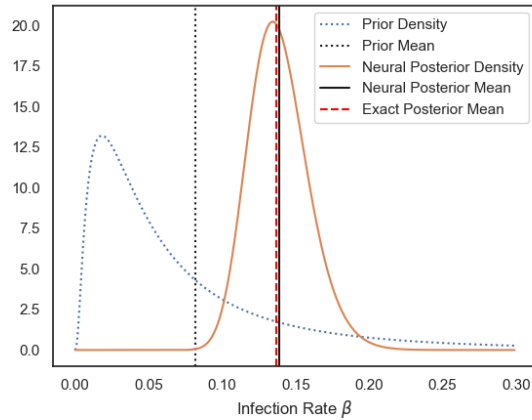


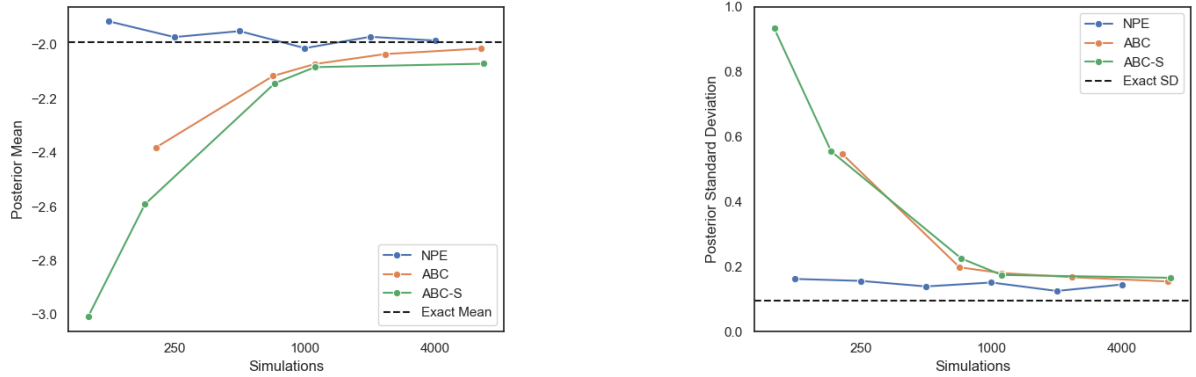
Figure 2: Comparison of lognormal prior and NPE-fitted approximate lognormal posterior for a homogeneous infection rate.

being a 52-dimensional vector, exists largely on a unidimensional subspace of  $\mathbb{R}^{52}$ ,<sup>8</sup> which would mean  $g(\mathbf{I})$  does not reduce the effective dimensionality of the simulated data.

Given even a few hundred training simulations, NPE yields highly-accurate approximations of the posterior infection rate. These approximations are nearly unbiased, with variances only slightly higher than the likelihood-based posterior. NPE is competitive with Rejection Sampling in terms of efficiency, despite being agnostic of the likelihood of parameter draws. In contrast, ABC requires exponentially more samples to converge on a quality approximation of the posterior: the NPE posterior estimate trained on 250 samples appears to be more accurate than the ABC estimate fitted with 4,000 (an acceptance rate of 2.5%). This suggests that 250 simulation samples are sufficient for NPE to learn the general posterior mean and variance, demonstrating the relatively quick convergence of a parametric estimator as compared to a nonparametric one.

The choice of prior impacts both the efficiency and accuracy of simulation-based posterior inference. In theory, a well-calibrated prior will result in a higher acceptance rate for ABC and more efficient training for NPE. In Figure 3.2, we compare the robustness of ABC and NPE posterior estimates are with respect to the choice of prior distribution. Both methods are fitted using only 500 simulated samples; as our ABC estimate, we keep the 100 samples closest to the observed data. First, we explore the effect of prior bias (Figure 4a): we consider several priors on  $\log(\beta)$  of the form  $\mathcal{N}(\mu_0, 1)$ , where  $\mu$  ranges from  $-4$  to  $-0.5$ . When  $\mu_0$  is small compared to  $\log(\beta)$  (i.e. downward-biased

<sup>8</sup>Roughly speaking, all feasible  $\mathbf{I}$  have a similar shape and live on a spectrum from flatter to steeper curves.



(a) Estimation of the posterior mean (log-scale) of the infection rate.

(b) Estimated posterior variance (log-scale) of the infection rate.

Figure 3: Comparison of the accuracy and sample efficiency trade-off of simulation-based inference. ABC-S denotes ABC using a summary statistic of the data; we show the exact (likelihood-based) posterior as a baseline.

prior), the resulting ABC estimates of the posterior distribution are heavily biased and high-variance. Interestingly, when  $\mu_0$  is upward-biased, the ABC estimate and NPE estimates are similar. This asymmetry is due to the nonlinear exponential transformation involved in moving from  $\log(\beta)$  to  $\beta$ . When  $\mu_0$  is small, the resulting prior draws  $\beta \sim \text{Lognormal}(\mu_0, 1)$  will all be close to zero and far from  $\beta^*$ , hindering the accuracy and efficiency of ABC. In contrast, NPE is robust with respect to choice of prior mean, yielding consistent estimates of posterior mean and variance for all settings of  $\mu_0$ . In effect, NPE can *generalize* a learned predictive model (i.e. what values of  $\beta$  are likely to give rise to an observed dataset  $\mathbf{I}$ ?) despite a relative lack of training data close to the true parameter value  $\beta^*$  and the observed data  $\mathbf{I}_o$ . Owing to the parametric assumptions on the form of the posterior, NPE can make efficient use of sparse simulated samples through extrapolation, whereas ABC depends on closely reproducing the observed data.

Figure 4b shows the effect of prior variance on ABC and NPE. In this experiment, we consider prior distributions on  $\log(\beta)$  of the form  $\mathcal{N}(-2, \tau_o^{-1})$ , where the prior *precision*  $\tau$  ranges from 1/16 to 16. A small value of  $\tau$  corresponds to a weak (high variance) prior, and a large value of  $\tau$  corresponds to a strong (low variance) prior. As with prior bias, the NPE posterior approximations do not change by much with respect to prior variance: whether the simulated training samples are all close to  $\mathbf{I}_o$  or are more widely dispersed, NPE can learn a good approximation to the posterior conditional on arbitrary data  $\mathbf{I}$ . By comparison, ABC’s performance suffers when the prior is diffuse. ABC posterior estimates exhibit high variance and some bias given a weak prior. The efficiency of ABC depends heavily on the choice of prior (a.k.a. proposal distribution), so an uninformative or miscalibrated prior combined with limited sample availability will result in a poor approximation of the posterior. Overall, Figure 3.2 shows that NPE is more robust than ABC when dealing with a lack of strong and/or accurate prior information.

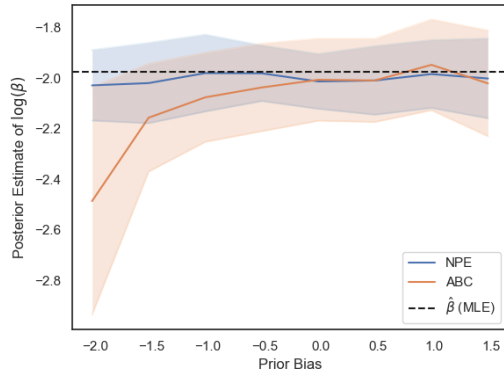
### 3.3 Experiment II: Heterogeneous Transmission

For our next set of experiments, we consider a facility with 5 floors and unknown, heterogeneous infection rates  $\beta$  varying within floors and between roommates; see Table 1 for the true parameter values. Estimating multiple location-based infection rates is considerably more challenging an inference problem than estimating a single infection rate, so to control the signal-noise ratio we increase the facility population size  $N$  to 300 while keeping all other fixed parameters the same as before.

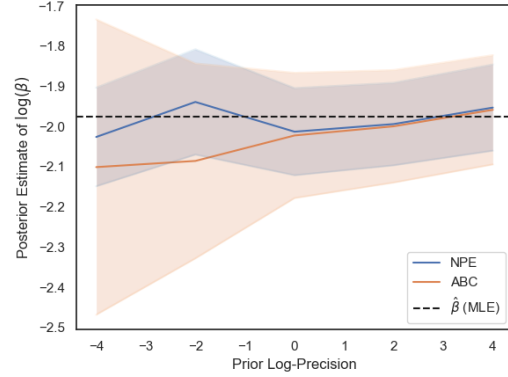
In Figure 5a, we plot the proportion of infected patients  $\tau$  over time across the facility as well as within each floor. The floor-level curves appear more volatile than the facility-level curve, which can be explained by the relatively smaller sample size, 60 patients per floor. We assign  $\beta$  a multivariate lognormal prior with a diagonal (uncorrelated) covariance structure:

$$\log(\beta) \sim \mathcal{N}(\boldsymbol{\mu} = -3, \boldsymbol{\Sigma} = I_7). \quad (18)$$

As before, we used Rejection Sampling to obtain a likelihood-based, ground-truth estimate of the posterior distribution  $p(\beta \mid \mathbf{X})$ . Despite the heterogeneous posterior having a dimension of only 7, Monte Carlo sampling is far more difficult than in the homogeneous case. Rejection Sampling required more than one million (!) draws from the prior to

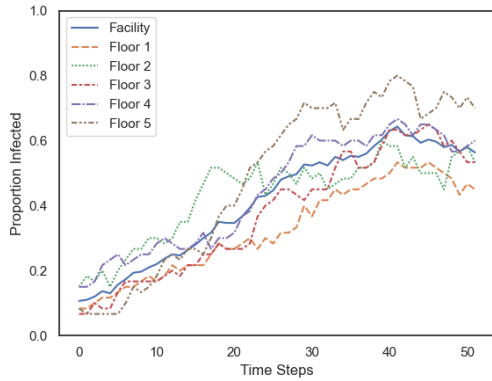


(a) Effect of prior bias on posterior approximation.

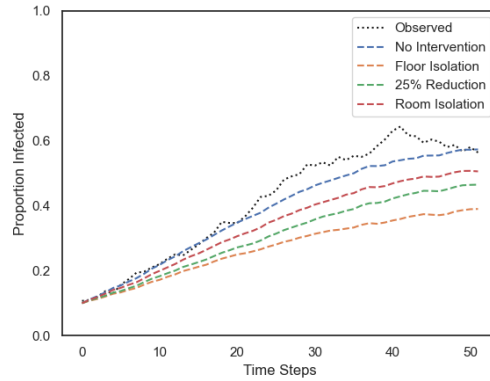


(b) The effect of prior precision ( $\log_2$  scale) on posterior approximation.

Figure 4: Robustness of NPE and ABC estimates of the homogeneous rate of infection with respect to choice of prior. The solid lines indicate the estimated posterior means and the shaded areas indicate one standard deviation of error. As an accuracy benchmark independent of the prior, plot the maximum likelihood estimate (MLE) of  $\beta$ .



(a) Observed proportion of infected patients over time for the entire facility and by floor.



(b) Impact of various interventions in the rate of transmission on the overall proportion of infected patients over time.

Figure 5: Visualizing a simulated outbreak under a stochastic susceptible-infected transmission model with heterogeneous rates of infection.

yield 100 accepted posterior samples.<sup>9</sup> For our simulation-based approaches to inferring the posterior, we constructed seven statistics or “views” of the data, each a location-specific time series corresponding to one of the parameters  $\beta_j$  in  $\beta$ . These are the overall infection case rate over time ( $\mathbf{I}$ ), the case rates by floor, and the proportion of rooms with both roommates infected. We denote these statistics collectively as  $\mathbf{J}$ , a vector of length 364 (7 times 52). For details on how we compute  $\mathbf{J}$  from  $\mathbf{X}$ , see Appendix C. Analogously to Equation 17, we aim to approximate

$$\hat{p}(\beta | \mathbf{J}) \approx p(\beta | \mathbf{J}) \approx p(\beta | \mathbf{X}) \quad (19)$$

whether by Monte Carlo sampling or by NPE.

Often, practitioners of variational inference make the mean-field approximation, i.e. they assume that the posterior is fully factorized with statistically independent components. When the variational family is Gaussian, this is equivalent to fitting a diagonal covariance matrix. This approximation is made for the sake of computational convenience: a diagonal covariance matrix has  $p$  parameters, whereas a full covariance matrix has  $(p^2 + p)/2$ . We fit both NPE with a full covariance matrix and NPE with the mean-field approximation in order to compare their efficiency (see Figure 3.3 below).

We found that directly fitting a multivariate normal (MVN) approximation to  $\beta$  via NPE rather than a multivariate lognormal approximation<sup>10</sup> resulted in improved estimation of parameters. While the lognormal NPE approximation yielded accurate point estimates of the infection rates, it misspecified the covariance structure, underestimating the negative posterior correlation between the facility rate  $\beta_0$  and the within-floor rates  $\beta_{1:5}$ . Intuitively, the facility rate and floor rates offer competing explanations for a given number of cases: if the floor rates are high, the facility rate must be low and vice versa. Empirically, the likelihood-based sample obtained via Rejection Sampling showed evidence of negative correlation (see Appendix E for a visualization). Additionally, the covariances appeared more Gaussian (i.e. elliptical correlations) on the natural scale rather than the log scale, suggesting that a lognormal posterior approximation is problematic for the heterogeneous SI model.

A MVN posterior approximation produced similarly accurate point estimates but exhibited lower posterior predictive uncertainty due to capturing the true posterior correlations (see Figure 6). One drawback of an MVN approximation is that it may put appreciable posterior density on negative rates, which are impermissible under our model assumption. To fix this problem, we can truncate the MVN approximation at zero, forcing all samples of  $\beta$  to be strictly positive. Truncated normal distributions can be harder to sample from, though our MVN estimates largely converged on positive values. We discuss the general problem of selecting the variational family for multidimensional posterior approximation in Section 5.

In Table 1, we compare approximate posterior mean point estimates of the heterogeneous infection rates obtained via NPE and ABC to the likelihood-based exact estimates. NPE and ABC were fitted with 4,000 and 7,646 simulation samples respectively. Despite ABC having access to nearly twice as many samples, the NPE point estimates are less biased on balance. In particular, the ABC estimate of  $\beta_5$ , the infection rate within floor 5, is rather inaccurate. We theorize that this is because the true posterior mean (0.107) for  $\beta_5$  lies at around the 80th percentile of the prior, meaning that the majority of proposed Monte Carlo draws of  $\beta$  underestimate the infection rate for floor 5.<sup>11</sup> We report estimated posterior standard deviations for each component of  $\beta$  in Table 2. The simulation-based, approximate posterior standard deviations are higher than their exact counterparts, which is expected since NPE and ABC estimate posterior distributions conditioned on descriptive statistics, which incur some loss of information. Nevertheless, for five out of the seven infection parameters, NPE exhibits lower posterior uncertainty than ABC (for the remaining two, they are virtually tied). Despite using nearly twice as many samples, ABC is limited to estimating an  $\epsilon$ -accurate approximation of the posterior, so it is unsurprising that it provides a looser fit of the parameters than an optimized multivariate Gaussian.

In Figure 3.3, we visualize the efficiency-accuracy trade-off of competing simulation-based inference methods. We fitted NPE using a full-covariance MVN approximation, NPE with a mean-field MVN approximation (denoted NPE-MF), and ABC. All methods were fitted using parameters  $\beta$  sampled from the prior and simulated  $\mathbf{J}$  (summary statistics of the data calculated from  $\mathbf{X}$ ), and we let the number of simulations used vary from 250 to nearly 8,000. In all subplots, we compare simulation-based posterior mean point estimates of infection rates against exact, likelihood-based estimates. In Figure 7a, we evaluate the total squared error across all 7 parameters. As a representative subset

<sup>9</sup>Markov Chain Monte Carlo (MCMC) would likely have been a more sample-efficient likelihood-based approach, but it has no guarantees of unbiased estimation if good mixing is not achieved. Hamiltonian Monte Carlo, a computationally faster variant of MCMC, requires knowing the gradient of the likelihood, which may be intractable (or undefined) in the case of complex simulation models.

<sup>10</sup>I.e., forgoing the log transformation entirely

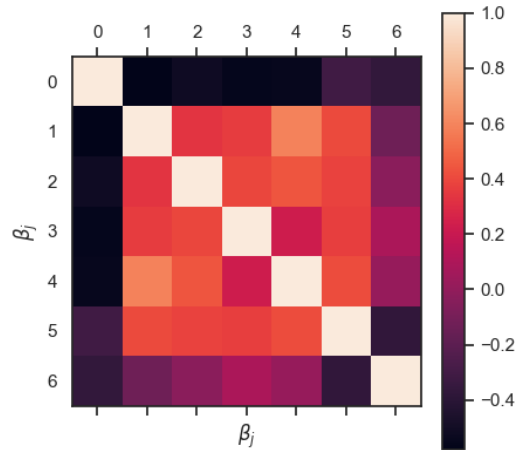
<sup>11</sup>This likely contributed to Rejection Sampling requiring more than a million samples: a prior even somewhat miscalibrated in a single dimension would result in many  $\beta$  draws of low likelihood.

Table 1: Posterior mean point estimates of heterogeneous infection rates.

Transmission Rate	Value	Exact Mean	NPE Mean	ABC Mean
Facility	0.05	0.0490	0.0517	0.0603
Floor 1	0.02	0.0210	0.0312	0.0303
Floor 2	0.04	0.0631	0.0448	0.0517
Floor 3	0.06	0.0432	0.0502	0.0406
Floor 4	0.08	0.0608	0.0664	0.0614
Floor 5	0.1	0.107	0.0980	0.0771
Room	0.05	0.0465	0.0414	0.0565

Table 2: Estimated marginal posterior standard deviations of heterogeneous infection rates.

Transmission Rate	Value	Exact SD	NPE SD	ABC SD
Facility	0.05	0.0132	0.0162	0.0215
Floor 1	0.02	0.0135	0.0226	0.0220
Floor 2	0.04	0.0198	0.0240	0.0333
Floor 3	0.06	0.0183	0.0237	0.0234
Floor 4	0.08	0.0223	0.0273	0.0321
Floor 5	0.1	0.0243	0.0276	0.0426
Room	0.05	0.0108	0.0235	0.0452

Figure 6: Correlation heatmap of heterogeneous infection rates  $\beta_j$  ( $j = 1, \dots, 6$ ), estimated via NPE using a MVN approximation.

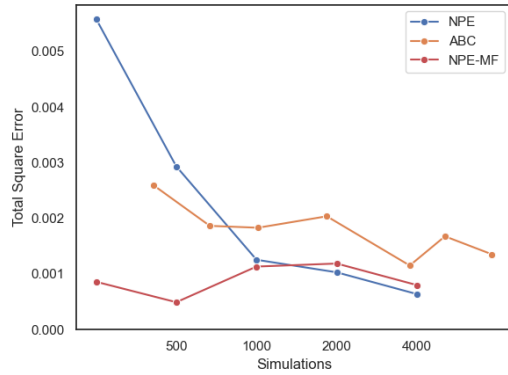
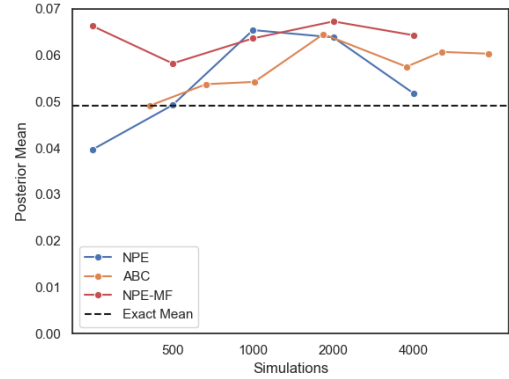
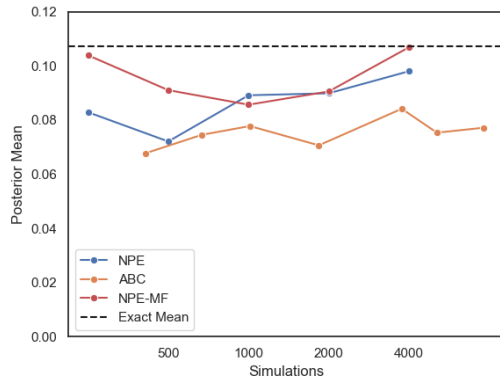
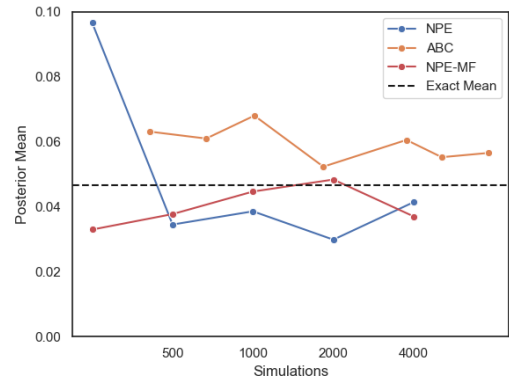
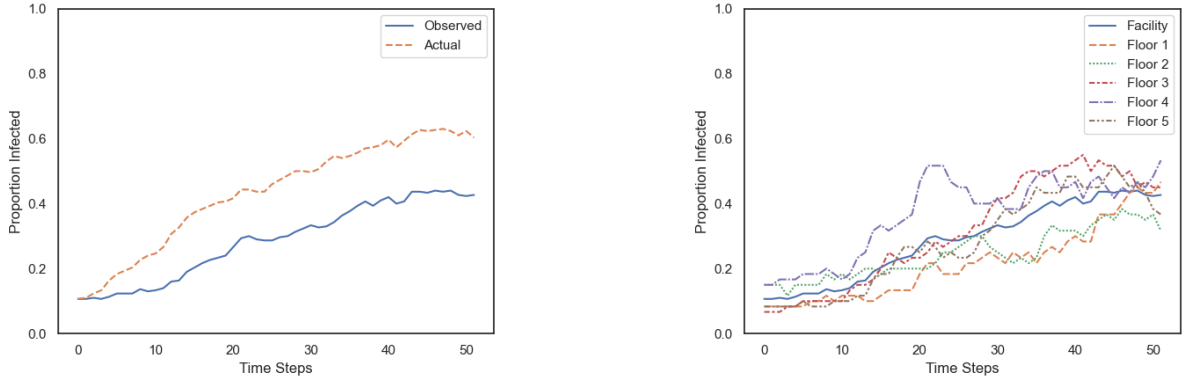
(a) Total squared error across all seven  $\beta_j$  in  $\beta$ (b) Estimation of the facility infection rate  $\beta_0$ .(c) Estimation of the infection rate within Floor 5,  $\beta_5$ .(d) Estimation of the infection rate between roommates,  $\beta_6$ .

Figure 7: Simulation-based estimation accuracy and sample-efficiency for heterogeneous infection rates. Likelihood-based posterior mean estimates are used as the baseline.

of the individual components of  $\beta$ , we also show the convergence of posterior mean estimates for the the facility rate  $\beta_0$  (Figure 7b), the rate for floor 5  $\beta_5$  (Figure 7c), and the room-level rate  $\beta_6$  (Figure 7d).

As Figure 3.3 shows, mean-field NPE is quite accurate when trained on even a few hundred simulations, reflecting that low-dimensional parametric optimization tends to be highly efficient. Given 1,000 or more simulations, full-covariance NPE is similarly accurate; more training data is required to estimate the posterior correlations. ABC gradually becomes more accurate as it is given more simulated (i.e., as  $\epsilon$  and the acceptance rate are reduced), though on balance it produces estimates more biased than NPE. For all settings of  $\epsilon$ , ABC struggled to accurately estimate  $\beta_5$ , which we attribute to the relatively greater distance of the marginal posterior from the prior. Once again, we see evidence that NPE can leverage regression modeling to learn the posterior from relatively scarce training samples, extrapolating beyond the *a priori* probable regions of the parameter space.

Fitting a mechanistic transmission model to a dataset allows an epidemiologist to reason about the behavior of an infection disease system under counterfactual interventions. For example, there might be interest in simulating what would happen to the case count over time if a hospital applied an intervention that halved the average rate of contact. After calibrating the model parameters to a dataset, we can simulate a counterfactual scenario by directly manipulating the force of infection (see Equation 8) and observing the resulting behavior of the posterior predictive mean distribution. In Figure 5b, we show the effect of several interventions. The blue line (“no intervention”) is the same as the original posterior predictive mean, which closely follows the observed data. We depict three counterfactual adjustments to the transmission model. “Floor isolation” depicts a reduction of inter-floor contact by 90%, representing a near-total quarantining of healthcare workers by floor. “Room isolation” entails eliminating the within-room additional transmission risk. Lastly, “25% reduction” represents an across-the-board decrease of infectious contact rates by one quarter. Floor isolation appears to decrease the number of infected patients more than the other interventions, suggesting that this



(a) Comparison of the observed (symptomatic) and actual proportion of infected patients over time with  $\eta = 0.1$

(b) Observed proportion of infected over time for the facility and by floor

Figure 8: Visualization of a simulated epidemic realization under an SI model with partial observation and heterogeneous transmission.

may be the most effective policy to reduce case burden in the facility. While we highlighted three relatively simple interventions, this predictive framework could be used to test a more extensive range of policies and more complicated scenarios.

### 3.4 Experiment III: Partial Observation

For our last simulated experiment, we turn to the problem of calibrating a stochastic model to a partially-observed epidemic. As we argued in Section 3.1.4, incomplete observation of infection times results in a model with a highly intractable likelihood function due to the large number of latent variables. However, forward simulation from such models is simple, and our previous experiments have shown that NPE accurately estimates model parameters from data simulation alone. With this in mind, we modify our previous simulation setup (Section 3.3) so that  $\eta = 0.1$ : that is, an expected 10% patients with asymptomatic colonization show observable symptoms of infection (see Section 3.1.4 for the details of this model).

In Figure 8a, we compare the observed case count over time to the actual number of infected patients. The former includes individuals who are screened upon arrival and colonized individuals who develop symptoms (with probability  $\eta$ ); the latter comprises both observed cases and asymptomatic but infectious carriers. By the end of the period of study, approximately 20% of patients in the facility are asymptotically colonized. The majority of infectious are observed throughout, despite  $\eta$  being close to zero. We show a breakdown of observed cases by floor with the facility-level case rate as a comparison in Figure 8b. One effect of partial observation is that the location-based heterogeneity in transmission is masked by a greater level of noise. For example, while Floor 3 has the third highest infection rate (see Table 3 for exact parameter values), for much of the period of observation, Floor 3 exhibits the highest infection burden.

To estimate the unknown infection rates, we fit ABC and NPE with a MVN posterior approximation to simulated data, using the same diagonal lognormal prior as in Section 3.3, which presupposes a mode of 0.0498 for each  $\beta_j$ . We used 4,000 samples to train NPE and took 100 ABC samples from 12,292 simulations. In Table 3, we compare the two methods' posterior mean point estimates and 90% (corresponding to the (0.05, 0.95) quantile range). The NPE mean estimates are overall close to the ABC estimates, despite NPE having been fit with less than one third of the samples. Both methods differentiate infection rates by floor, roughly by the observed infection burden (cf. Figure 8b), e.g. returning smaller estimates for Floors 1 and 2 and a higher estimate for Floor 4. For  $\beta_1$ ,  $\beta_2$ ,  $\beta_5$ , and  $\beta_6$ , the NPE posterior estimate places a non-trivial amount of posterior density below zero, as zero is contained within these 90% credible intervals. This reflects high posterior uncertainty—to be expected in a partially-observed system—since non-positive values are never drawn from the lognormal prior. As negative infection rates are inadmissible under our model assumptions, we can treat these credible intervals as an ad hoc Bayesian significance test: given our prior, the NPE estimate suggests that we do not have sufficiently strong evidence to suppose that  $\beta_1$ ,  $\beta_2$ ,  $\beta_5$ , and  $\beta_6$  are non-zero. Though we know that this isn't the case, we could interpret this result as motivating a more parsimonious model, with a facility-level infection rate and elevated rates of transmission within floors 3 and 4.

Table 3: Inference of heterogeneous infection rates in a partially observed outbreak. For both ABC (12,292 samples) and NPE (4,000 samples), we report the estimated posterior mean and a 90% credible interval.

Transmission Rate	Value	NPE Mean	NPE CI	ABC Mean	ABC CI
Facility	0.05	0.0615	(0.0279, 0.0951)	0.0555	(0.0232, 0.0981)
Floor 1	0.02	0.0215	(-0.0235, 0.0665)	0.0332	(0.00604, 0.0729)
Floor 2	0.04	0.0313	(-0.0214, 0.0839)	0.0346	(0.00862, 0.0753)
Floor 3	0.06	0.0825	(0.0200, 0.145)	0.0685	(0.0177, 0.152)
Floor 4	0.08	0.0987	(0.0223, 0.175)	0.0923	(0.0226, 0.186)
Floor 5	0.1	0.0349	(-0.0325, 0.102)	0.0555	(0.0104, 0.110)
Room	0.05	0.0565	(-0.0112, 0.124)	0.0661	(0.0114, 0.177)

In the absence of a likelihood-based posterior estimate, posterior predictive checks are a reasonable benchmark for how well NPE and ABC calibrate the heterogeneous infection rates under partial observation. To obtain a posterior predictive distribution under NPE, we truncate the approximate MVN posterior below zero, using rejection sampling to obtain a posterior sample of strictly positive  $\beta$ . In Figure 8, we visualize three posterior predictive checks for  $\beta_0$ ,  $\beta_5$ , and  $\beta_6$  as a representative subset of  $\beta$ . For all  $\beta_j$ , the NPE posterior predictive mean closely coincides with the ABC posterior predictive mean, and generally these means closely interpolate the observed data.<sup>12</sup> While we do not visualize individual posterior predictive draws for ABC, the variation of both distributions are quite similar. Despite the similarity of the *marginal* simulation-based posterior approximations, NPE estimates a sharper and more structured covariance than ABC, that is, stronger positive correlation between the floor-level infection rates, and more negative correlation between  $\beta_0$  and the location-specific parameters. For the respective correlation heatmaps, see Appendix E.

## 4 CRKP Case Study

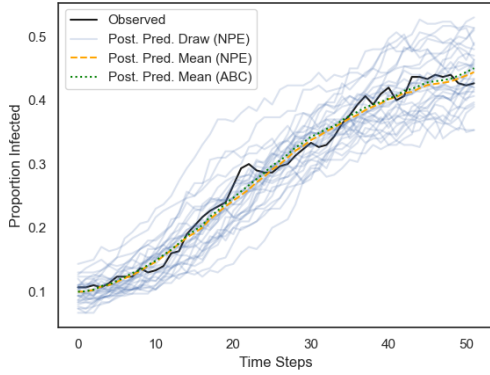
Having shown that simulation-based inference can be used to calibrate our stochastic epidemic model for HAIs to spatially structured data, we turn our attention to an empirical study of carbapenem-resistant *Klebsiella pneumoniae* (CRKP) transmission in a long-term acute care hospital (LTACH) in Chicago, Illinois. *Klebsiella* is a bacterium that originates in human feces and typically spreads through (possibly indirect) skin contact between humans. It generally is an asymptomatic colonizer in healthy individuals, but if it penetrates into internal organs, it can erupt into a life-threatening infections such as pneumonia or sepsis. Due to its prevalence in the healthcare system, CRKP is a major threat to public health (Karampatakis, Tsergouli, and Behzadi 2023). LTACHs are major breeding sites for strains of HAIs such as CRKP that are resistant to commonly-used antibiotics, making them difficult to treat. LTACH patients, who receive intensive treatment over extensive periods of time, are often among the sickest-of-the-sick within the healthcare system. They are triply vulnerable to invasive infection, due to their immunity being weakened, being administered invasive, indwelling devices, and having frequent exposure to healthcare workers serving many high-risk patients.

A noteworthy feature of our CRKP dataset, which we describe in detail in Section 4.1 is that it arose from an *prospective* study of infection. Patients at a healthcare facility are usually tested for CRKP and similar pathogens upon admission (i.e. patient screening) and in cases of symptomatic, invasive infection. This practice would likely miss many patients—perhaps a majority—who are asymptotically colonized with CRKP yet still infectious. This makes it significantly easier to model infectiousness, though we consider this analysis to be a prototype that could be extended to more typical settings with incomplete or irregular observation of event times. To model the spread of CRKP through the LTACH at an individual level, we adapt the stochastic SI model we introduced in Section 3, and we outline these modifications in Section 4.2. Our principal motivating research question in this analysis is whether CRKP transmission risks in this facility are spatially structured.

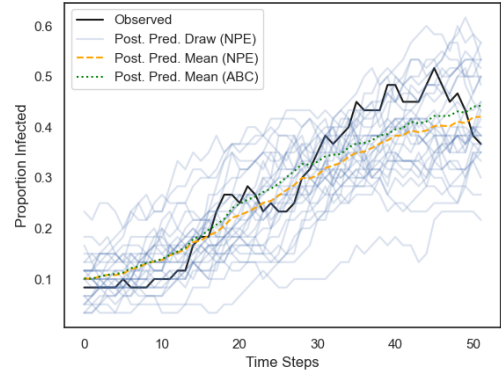
### 4.1 CRKP Dataset

A Chicago-area LTACH carried out an intervention attempting to reduce CRKP transmission over the course of a single year, from June 2012 to June 2013. As part of this effort, every patient in the facility was tested for CRKP every other week after they were admitted (Hawken et al. 2022), which in addition to the usual screening upon intake amounts to near-complete observation of cases. Over the course of the intervention, infected patients were geographically

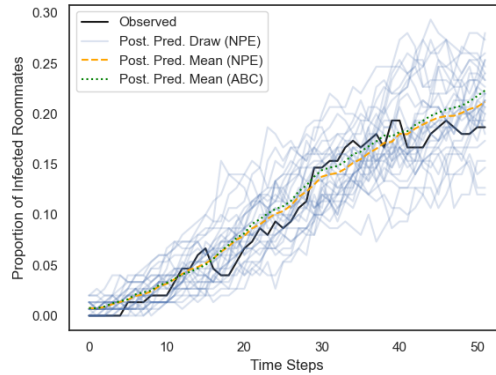
<sup>12</sup>The simulation-based posterior predictive means respectively overestimate and underestimate the case incidences for Floors 1 and 4. This is not necessarily a sign of miscalibration: rather, we can treat these as predictions of how many infected patients we’d expect to see given  $\eta = 0.1$ . We could also see this as the effect of shrinkage towards the prior we set on  $\beta$ .



(a) Posterior predictive check of  $\beta_0$  with respect to the facility-level infection incidence.



(b) Posterior predictive check of  $\beta_5$  with respect to the infection incidence on Floor 5.



(c) Posterior predictive check of  $\beta_6$  with respect to the fraction of rooms with multiple infected patients.

Figure 9: Posterior predictive checks for three infection rate parameter in the partially-observed SI model. For each variable, show 30 NPE posterior predictive draws of the relevant observable, the NPE posterior predictive mean, and the ABC posterior predictive mean.

isolated in ward cohorts, all patients were administered daily baths of chlorhexidine gluconate (an antiseptic agent), and healthcare workers received additional training and monitoring.

In addition to test results, the dataset includes the time of admission and discharge for each patient as well as the floor(s) and room(s) in which they stayed during their visit. We refer to location information as patient “trace data.” Overall, the dataset describes 890 patients and 1,112 distinct visits, with 18% of patients making two or more visits to the facility. Patients resided in five floors<sup>13</sup> and 95 rooms; in many cases, patients move between multiple floors and rooms over the course of one visit. 259 (29%) patients tested positive for CRKP at some point. The median length of a single visit was 24 days, while less than one in seven visits were shorter than a week. 95% of patients are tested within the first three days of their stay. We assume that a positive test within three days of admission means a patient entered the facility already colonized with CRKP and that CRKP cannot be acquired from another patient until at least the fourth day of a visit.

Though the original data is recorded on a day-by-day frequency, we resample to a weekly resolution. This smooths and reduces the dimensionality of the data without erasing fluctuations over smaller timescales, since the vast majority of patient stays last longer than a week. In Figure 10a, we visualize a breakdown of the population of the LTACH over time. We see that the total patient population generally fluctuates between 110 and 120 per week, with around 20 new patients admitted per week. About 50% of patients are colonized with CRKP at the start of the study, and this proportion decreases somewhat over the course of the study, suggesting that the intervention was modestly effective.

<sup>13</sup>(We treat the Special Care Unit, or SCU, as a floor, consistent with how the trace data is encoded.)

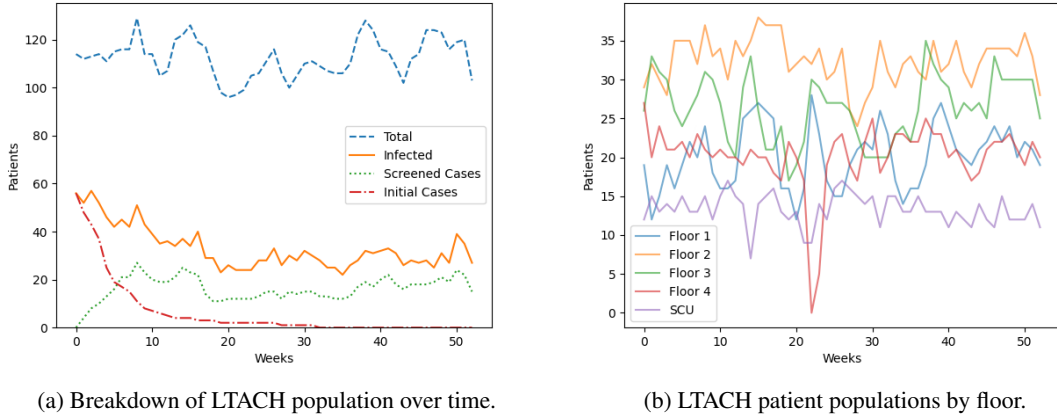


Figure 10: Visualizing the LTACH CRKP Dataset

We also show the group of patients who were infected at the start of the study; by week 10, these patients have been mostly discharged. Lastly, we show the number of patients who screen positive for CRKP upon admission during the study. For most of the period of observation, the majority of CRKP cases come from outside the facility (i.e. are screened), implying that within-facility transmission contributes less to the overall incidence rate. We show a breakdown of patient population (both colonized and uncolonized) by floor in Figure 10b. Floor populations are generally stable, but the population of floor 4 temporarily plummets to zero around week 20. Given the coinciding spike in population of Floor 1, it is possible that this is an issue of data sanity, though the overall facility population appears to drop around week 20.

## 4.2 CRKP Transmission Model

We assume that patients are either uncolonized with CRKP (susceptible) and colonized (infected), and that recovery does not occur. To model the spatially-heterogeneous spread of CRKP within the LTACH, we use a stochastic, discrete time SI model adapted from the one described in Section 3 with a few modifications. In our simulation experiments, we randomly modeled the turnover of patients (3.1.2). In our CRKP study, however we know the exact day that patients enter and leave the LTACH along with their test results for CRKP upon arrival. We therefore treat patients' visit times and external CRKP infections as fixed conditions of the simulation model. In other words, we only simulate the possibility of a patient getting CRKP *within the facility*, based on the (possibly individualized) time-varying force of infection. Likewise, we no longer randomly sample the event that a patient enters the facility infected or susceptible but instead treat these events as fixed based on the available admissions screening data.

The CRKP study tracks  $N = 890$  distinct patients over the course of  $T = 53$  weeks. As before, let  $\mathbf{X}$  be an  $N \times T$  matrix of patient infection status, with  $X_t^{(i)}$  equaling one if patient  $i$  is infected with CRKP at the start of week  $t$  and zero otherwise.<sup>14</sup> We can think of  $\mathbf{X}$  as the output of the simulation, though we summarize  $\mathbf{X}$  e.g. through the overall case count  $\mathbf{I}$  and location-specific statistics (see Appendix C). For fixed simulation parameters, we let the  $N \times T$  matrices  $\mathbf{W}$ ,  $\mathbf{F}$ , and  $\mathbf{R}$  denote the facility trace, floor trace, and room trace respectively. For the facility trace,  $W_t^{(i)}$  equals one if patient  $i$  is present in the facility during week  $t$  and zero otherwise. Lastly, let  $\mathbf{V}$  record screening results: for a patient  $i$  newly admitted to the facility at time  $t$ ,  $V_t^{(i)}$  equals one if the patient tests positive for CRKP during screening and zero if that patient has a negative result. As with the simulation experiments, we compute the force of infection based on a homogeneous infection rate  $\beta$  or a vector of heterogeneous infection rates  $\beta$  of length seven (a facility rate, five floor rates, and a room-level rate) (see Equation 8). We write out the simulation procedure in Algorithm 4.

## 4.3 Results

From Figure 10a, we can see that in most weeks the majority of cases originate from outside of the facility. At no point does the number of infected patients make up a majority of patients in the facility, nor is there a long-term upward trend in case burden. We can surmise that a high rate of patient turnover counterbalances any accumulation of infection.

<sup>14</sup>In this case,  $i$  indexes individual patients and not fixed locations.

**Algorithm 4** CRKP Transmission Simulator

---

**Input:** Vector of transmission rates  $\beta$ , facility trace  $\mathbf{W}$ , floor trace  $\mathbf{K}$ , room trace  $\mathbf{R}$ , screening results  $\mathbf{V}$

**Output:**  $N \times T$  matrix  $\mathbf{X}$  of infection logs  $\mathbf{X}^{(i)} = \{X_1^{(i)} \dots X_T^{(i)}\}$  for all patients  $i = 1, \dots, N$

```

for  $t = 1, 2, \dots, T$  do
  for  $i \in 1, \dots, N$  do
    if  $W_t^{(i)} = 1$  and  $W_{t-1}^{(i)} = 0$  (or  $t = 1$ ) then                                ▷  $i$  is newly admitted
      Set  $X_t^{(i)} = V_t^{(i)}$                                                                                               ▷ screening results are fixed
    else
      if  $W_t^{(i)} = 1$  and  $W_{t-1}^{(i)} = 1$  then                                ▷  $i$  has stayed at least one week
        if  $X_{t-1}^{(i)} = 0$  then                                                                                          ▷  $i$  is susceptible
          Compute the individualized force of infection  $\lambda_i(t)$ 
          Draw  $X_t^{(i)} \sim \text{Bernoulli}(1 - e^{-\lambda_i(t)})$ 
        else
           $X_t^{(i)} \leftarrow 1$ 
        end if
      else
        Set  $X_t^{(i)} = \emptyset$                                                                                               ▷  $i$  is not present at time  $t$ 
      end if
    end if
  end for
end for

```

---

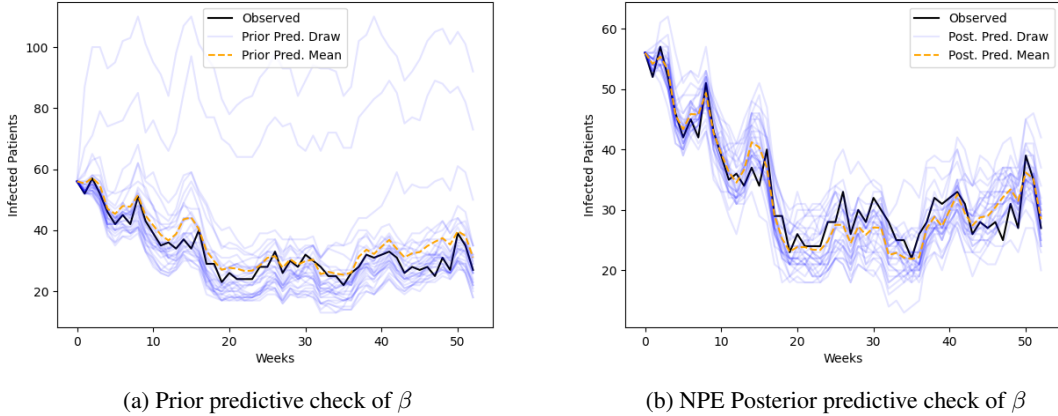


Figure 11: Predictive checks for the homogeneous CRKP infection rate

Based on what we observe at a glance, it is reasonable to ask whether there is significant risk of patient-to-patient CRKP transmission *within* the LTACH.

In our first experiment, we fit a homogeneous SI model to the CRKP data using NPE. We suppose that the infection rate has the prior  $\beta \sim \text{Lognormal}(\mu = -2, \sigma = 1)$ . This is a somewhat conservative prior that presumes a low overall infection rate. A prior predictive check over the facility-level incidence (Figure 11a) shows that this prior is well-calibrated to the data. Most prior predictive draws underestimate the observed incidence, although a few greatly overshoot it, illustrating the nonlinearity, unstable dynamics of the stochastic SI model. We trained NPE on 4,000 simulations to learn a lognormal approximation to the posterior homogeneous infection rate. We estimated that  $p(\beta | \mathbf{X}) \approx \text{Lognormal}(\mu = -2.06, \sigma = 0.124)$ , with a posterior mean of 0.129 and a 90% credible interval of (0.104, 0.157), suggesting statistically significant risk of patient-to-patient transmission within the facility. A posterior predictive check (Figure 11b) shows that this approximate posterior is well-tuned to modeling the overall incidence of CRKP within the LTACH. However, when case counts are stratified by location within the LTACH, the homogeneous model shows problematic behavior. In particular, the calibrated homogeneous model overestimates the CRKP incidence in Floors 2 and 4 and somewhat underestimates it in Floor 3. See Figure 18g in Appendix E for the complete set of posterior predictive check across locations.

Table 4: NPE (4,000 samples) and ABC (10,628) posterior estimates of heterogeneous infection rates for the CRKP dataset.

Rate	NPE Mean	NPE CI	ABC Mean	ABC CI
Facility	0.0420	(0.0234, 0.0678)	0.0411	(0.00990, 0.0846)
Floor 1	0.134	(0.0351, 0.323)	0.108	(0.0109, 0.294)
Floor 2	0.0457	(0.00842, 0.126)	0.0585	(0.00617, 0.150)
Floor 3	0.139	(0.0618, 0.259)	0.196	(0.0546, 0.330)
Floor 4	0.0337	(0.00585, 0.0946)	0.0547	(0.00664, 0.129)
SCU	0.0717	(0.00880, 0.223)	0.0764	(0.0110, 0.211)
Room	0.0846	(0.00767, 0.281)	0.123	(0.0103, 0.389)

We then fit a heterogeneous transmission model to the CRKP data, with an unknown vector of infection rates  $\beta = \beta_1, \dots, \beta_7$ , corresponding to a facility rate, five within-floor rates, and a room-level rate. For our prior, we suppose  $\beta_j \sim \text{Lognormal}(-3, 1)$  for all  $j$ . This prior assumes no correlation between components of  $\beta$  and a mode of 0.0498. We trained a neural network on 4,000 simulations from the heterogeneous SI model to fit a multivariate lognormal approximation to the posterior  $p(\beta | \mathbf{X})$ . Posterior predictive checks (Figure 14) show that the fitted heterogeneous model accurately predicts observed floor-level and facility-wide CRKP incidence. Interestingly, the heterogeneous model predicts slightly fewer cases overall than the homogeneous model (compare Figures 14a and 11b). The heterogeneous model appeared to do an adequate job of capturing room-level transmission (Figure 14d), somewhat underestimating the number of rooms with multiple infected roommates around weeks 25 and 40.

In Figure 12, we overlay the prior distributions (blue) and approximate posterior distributions (orange) for each component of  $\beta$  on the log-scale; all distributions shown are Gaussian. For the facility-level rate  $\beta_0$  and the rate for Floor 3 (and to a lesser extent, Floor 1) the posteriors are relatively narrow (low-variance) relative to the prior, indicating low posterior uncertainty for these components. The results suggest that there is an elevated risk of infection on Floors 3 and 4, and that there is some evidence of lower-than-expected CRKP transmission on Floors 2 and 4. These findings make intuitive sense: Floor 2 has the highest population of any floor (Figure 10b) but a rather low incidence of CRKP (Figure 14b, whereas on Floor 3, a slight majority of patients are infected with CRKP in a typical week.<sup>15</sup> For the SCU-level rate and the infection rate between roommates, the prior and posterior overlap completely, reflecting high posterior uncertainty, or equivalently, a lack of information on these rates in the data. Unsurprisingly, the SCU had the lowest weekly population of any floor, while within-room transmission is a very noisy phenomenon since virtually all rooms contained no more than two or three patients at any time.

As a point of comparison, we fitted an ABC approximation to the heterogeneous posterior, constructing an approximate posterior sample of size 100 from 10,628 simulations, an acceptance rate of less than 1%. We compare the posterior mean estimates and 90% credible intervals for the heterogeneous CRKP infection rates found by NPE and ABC in Table 4. The NPE and ABC results are generally similar: the ABC estimated rate is the highest by far for Floor 3, somewhat high for Floor 1, and relatively low for floors 2 and 4, and the estimated facility-wide infection rate is nearly the same for both NPE and ABC (0.0420 vs 0.0411). Except for the SCU- and room-level infection rates, the NPE marginal posteriors are a bit narrower, suggesting higher posterior uncertainty for ABC, which may be a result of approximation error. Analogously to Figure 12, we overlay the ABC posterior histograms over the prior densities in Figure 19 (see Appendix E). We found that ABC detected a strong posterior signal for only the Floor 3 infection rate. While the ABC and NPE point estimates differ slightly, we found that they yielded similar posterior predictive distributions for both the facility-wide CRKP incidence and the location-specific incidences (see Figure E in Appendix E).

Having calibrated a heterogeneous transmission model to the CRKP dataset, we experimented with various interventions to reduce the incidence rates. We illustrate two of these interventions in Figure 13. We estimated the effect of these interventions by calculating the resulting posterior predictive mean from simulations. For comparison, we also plot the factual posterior predictive mean (“No Intervention”) and the incidence had there been zero transmission within the facility (i.e. only CRKP cases from the outside). Reducing the rate of contact between individuals from different floors by 90% (“Floor Isolation”) did not appreciably reduce the predicted number of cases over time. However, reducing contact by 50% in the two floors with the highest infection rates (“Target Floors 1 & 3”) resulted in a significant decrease in CRKP incidence over time. The outcomes of these interventions suggest that transmission between patients within these two floors is the primary cause of the observed CRKP infections acquired within the LTACH.

<sup>15</sup>We surmise that, as part of the intervention against CRKP, infected patients were isolated in Floor 3.

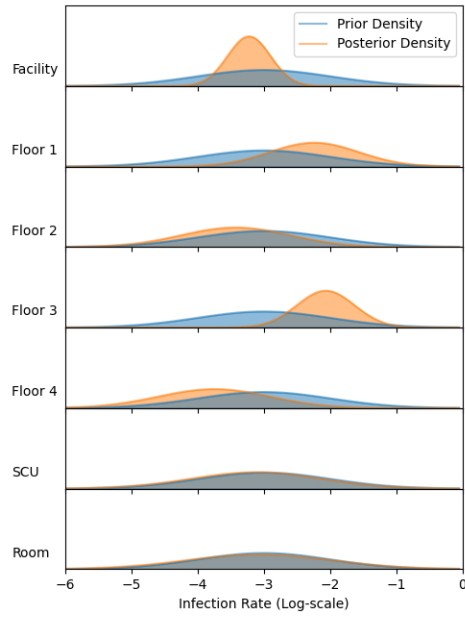


Figure 12: Comparison of priors and NPE posteriors for each component of  $\beta$ .

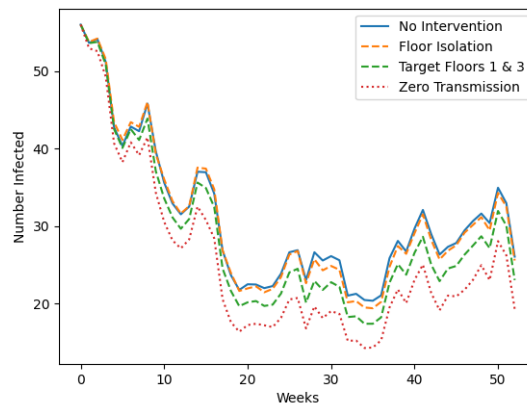


Figure 13: The simulated effect of transmission interventions on the overall incidence of CRKP.

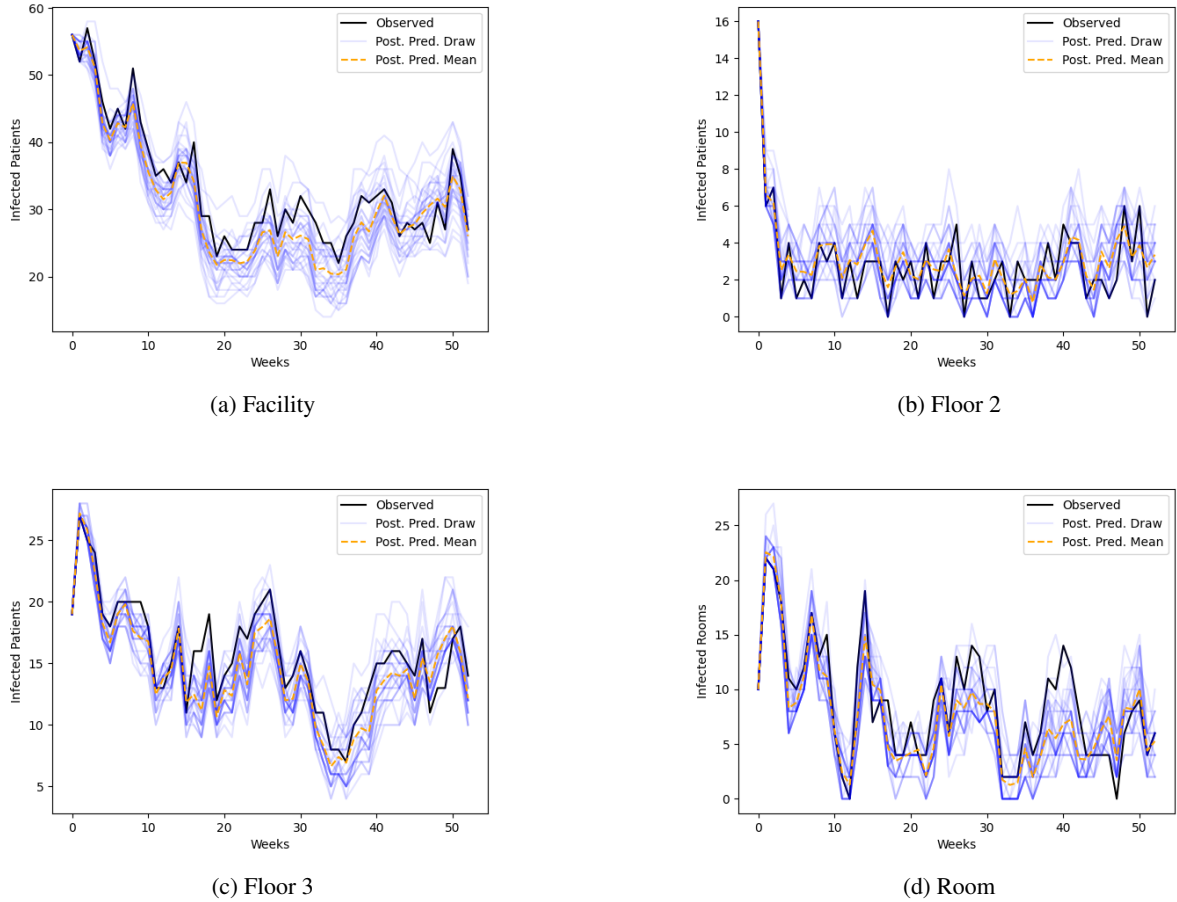


Figure 14: Selected posterior predictive checks for the heterogeneous CRKP infection rates estimated by NPE. See Appendix E for the complete set.

## 5 Discussion

Our simulation experiments tested the efficacy of simulation-based approaches to calibrating stochastic infectious disease models of increasingly complexity to epidemiological data. Where possible, we used exact, likelihood-based posterior estimates as a benchmark for simulation-based inference. We considered three estimators of the posterior that rely on independent parameter draws from the prior: Rejection Sampling (likelihood-based Monte Carlo sampling), ABC (simulation-based Monte Carlo sampling), and NPE (simulation-based parametric optimization). In this respect at least, these methods are simpler and more robust than MCMC and its variants, which depends on achieving adequate mixing (i.e. ergodicity) within the sampling chains. While it is not always straightforward to compare NPE to Monte Carlo sampling,<sup>16</sup>our results suggest that NPE comes close to likelihood-based inference in accuracy while making much more efficient use of simulated samples than ABC.

Particularly for Bayesian models with many unobserved parameters or latent variables, NPE demonstrates computational advantages as a tool for inference. It is not immune from the curse of dimensionality, however: NPE’s convergence was more irregular in the case of heterogeneous infection rates (Figure 3.3) than in the case of a single infection rate (Figure 3). NPE entails training a neural network to minimize the NPE loss objective (Equation 3), which relies on a Monte Carlo approximation (Equation 4) that may exhibit significant sampling error in high dimensional space. The efficiency of NPE is dependent on the choice of variational approximation: we saw that a fully factorized (mean-

<sup>16</sup>For example, Papamakarios and Murray (2016) compute the posterior log probability of the true parameters for ABC by fitting a Gaussian to the ABC nonparametric sample, comparing this against the NPE log probability. This mode of comparison is inherently favorable to NPE, since ABC is not designed to produce a Gaussian approximation. To an extent, NPE and ABC are apples and oranges.

field) posterior approximation produces accurate point estimates of the heterogeneous infection rates when available simulations are restricted. Conversely, when estimating a full covariance matrix, NPE appeared to perform worse than ABC in the lower limit while showing better asymptotic convergence. Simulated data is in some respects an ideal setting for neural networks: a lack of available training data is never a bottleneck, and provided the model  $p(\theta, \mathbf{x})$  is a decent fit for the data, NPE is always performing in-distribution prediction.

Papamakarios and Murray (2016), in their pioneering work, argued that NPE is efficient in comparison to ABC due to strong, parametric assumptions on the form of the posterior, reducing the dimension of the estimation problem. If the general (amortized) posterior has an a form that is reasonably regular with respect to the observed data, then NPE can interpolate the true posterior from a few training examples. This article offers a different, yet complementary perspective: NPE is efficient because it is *robust to the choice of prior*. As a regression technique, NPE can learn to extrapolate the conditional dependency of  $\theta$  on  $\mathbf{x}$  to regions where there is low prior density (e.g. Figure 4a). When the prior (proposal) is close to the posterior, ABC can be highly efficient, since draws are more likely to be accepted. In real problems, most priors are wrong, and so ABC will inevitably “waste” many simulation samples.

From a hypothesis testing standpoint, we believe that NPE may be sensitive to posterior signals that depart from the prior, whereas ABC can yield estimates overly biased to the proposal distribution. For instance, in our heterogeneous model simulation experiments (Section 3.3), NPE was better able to distinguish the floor that had the highest infection rate (c.f. Table 1). This is a particularly useful property for an estimator when employing strong priors or dealing with weak signals, as may often be the case in epidemiological models with complex, variegated transmission mechanisms.

A key challenge of using NPE is choosing the right variational approximation to the posterior. The Bernstein-von Mises theorem provides one argument why Gaussians combined with necessary parameter transformations may be good enough in practice for a wide range of problems: under some basic regularity conditions, a posterior distribution will converge on a normal (or multivariate normal) distribution as the observed sample size  $N$  increases (Gelman, Carlin, et al. 1995).<sup>17</sup> However, the situation commonly arises where normal approximations are more accurate for *marginal* distributions than the full joint distribution (Gelman, Carlin, et al. 1995).<sup>18</sup> We saw this phenomenon in our experiments with the heterogeneous SI model (c.f. Figure 3.3). The mean field approximation can be a useful for point estimates of parameters, yet posterior correlations often convey significant information about the data. We found that working with a untransformed multivariate normal worked somewhat better than a multivariate lognormal for modeling the full joint posterior distribution of  $\beta$  in our simulation experiments, but we were able to validate our choice of variational distribution against a likelihood-based posterior sample. These likelihood-based estimates are obviously hard to obtain in the problems where one would use simulation-based calibration. ABC may be a useful check on the approximate shape of the posterior, though ABC estimates may be too crude to accurately depict posterior correlations. Another solution is to employ a more flexible class of conditional density estimator (e.g. Normalizing Flows), though these introduce more (hyper)parameters, making them harder to train and interpret.

The findings from our empirical study of CRKP transmission in a Chicago-area LTACH offer some evidence that transmission risks vary with respect to a spatially-structured contact network across floors, though surprisingly we found no evidence of increased risk of transmission between roommates. A comparison of posterior predictive checks between the calibrated homogeneous and heterogeneous models suggested that

Though we compared posterior predictive checks between the homogeneous and heterogeneous models, we did not conclude whether the transmission was truly heterogeneous due to the difficulty of Bayesian model selection in the simulation-based setting (see Section 6). As part of the intervention, whole-genome sequencing (WGS) was conducted on all detected CRKP cultures. We did not make use of this data, though we hypothesize that the similarity between two strains, measured via single nucleotide polymorphism (SNP) distance conveys additional information on individualized transmission risks, e.g. by ruling out the possibility of transmission between two individuals infected with CRKP strains belonging to different clusters. We leave the problem of calibrating an epidemiological-genomic simulation model of HAIs for a future work.

## 6 Conclusion

We have demonstrated how NPE can be an effective yet simple method for calibrating stochastic epidemic models to data via simulation. NPE conserves computational time without demanding more human engineering effort than established statistical algorithms such as MCMC and ABC in its most basic form. While deep learning has not been

<sup>17</sup>This distribution will have a mean vector corresponding to the posterior mode(s) (MAP estimates) and a precision matrix corresponding to the observed information, i.e. the negative Hessian matrix for the (unnormalized) posterior evaluated at the mode.

<sup>18</sup>A marginal distribution is by definition an integral (i.e. summation) of the joint distribution, so the CLT implies that marginals will generally look more Gaussian than the joint.

widely adopted in the field of epidemiology, we believe this work shows how it can be of use to scientific modeling of complex transmission mechanisms and analyzing partially-observed epidemic data.

Our work has focused on the problem of Bayesian model calibration and parameter estimation, taking one model to be true, but this is only the first level of Bayesian inference. The second level is *model comparison* (MacKay 1992). For example, we might ask whether a heterogeneous transmission model better describes an outbreak than a homogeneous one. Because of its computational efficiency, NPE presents a viable way to rapidly “prototype” and compare many different models. However, rigorous, quantitative comparison of models is challenging in the simulation-based inference setting. Bayes factors, which naturally penalize more powerful (flexible) models, are the classical tool for Bayesian model comparison, but these depend on a model’s marginal likelihood (a.k.a. evidence),  $p(\mathbf{x}_o) = \int p(\mathbf{x}_o | \boldsymbol{\theta})p(\boldsymbol{\theta})d\boldsymbol{\theta}$ . Clearly, if the likelihood density is intractable, the evidence is hard to estimate. There has been some work on model selection for simulation-based inference for both ABC (Toni and Stumpf 2010; Robert et al. 2011) and neural density estimation (Spurio Mancini et al. 2023), but this remains a challenging problem. There is a need for further development of a complete “Bayesian Workflow” (Gelman, Vehtari, et al. 2020) for simulation-based inference that includes rigorous techniques for model diagnosis and comparison.

There has been proliferation in recent years of multiple data sources giving insight into the transmission of bacterial HAIs such as CRKP and MRSA. Clinical data collected within facilities, in addition to tracing the movement of patients over time and describing a dynamic contact network, also include information on the usage of indwelling devices, comorbid conditions, and symptomatic illness, all of which can inform transmission studies. Additionally, the decreasing cost of whole genome sequencing (WGS) has made it easier to identify potential transmission links between cases and to track infection between healthcare facilities. Bacteria such as CRKP evolve relatively slowly compared to their transmission, so it is often possible to divide a population of pathogens into distinct clusters. In a future work, we plan on extending our SI model for HAIs to simulate clustering of cases, which will provide valuable clues to individual-level transmission in more general healthcare settings where surveillance of pathogens is not prospective (Hawken et al. 2022). Other extensions of our model include modeling infection risk based on individual patient covariates and integrating transmission dynamics from multiple separate facilities.

While this work has focused on healthcare associated infections as a proving ground for simulation-based inference, our methodology could be applied to a wide range of epidemiological problems. One logical extension would be to use NPE for calibrating stochastic compartmental models with more states than the SI model, e.g. the Susceptible-Exposed-Infected-Recovered (SEIR) model. These introduce more unobserved, latent variables in the data generation process, which makes classical likelihood-based inference even more challenging. Fitting more capacious, flexible infectious disease models also motivates a rigorous Bayesian model selection procedure for simulators. Another use case for NPE would be to model diseases with strong temporal effects at multiple resolutions, such as influenza and measles. Time series data feature prominently in epidemiology, suggesting that sequentially-aware neural network architectures such as Recurrent Neural Networks or Transformers may be effective encoders in the NPE framework, bypassing the need to summarize high-dimensional time series data by hand. For many epidemiological problems, we believe that an explanatory, machine-learning based workflow can complement existing practices of mathematical modeling and established statistical tools for parameter inference.

## 7 Acknowledgements

We thank Declan MacNamara for technical advice on NPE and Hannah Steinberg for help interpreting the Chicago CRKP data. This work was supported by a Propelling Original Data Science (PODS) grant from the Michigan Institute for Data and AI in Society (MIDAS).

## References

- Ross, Ronald (1911). *The Prevention of Malaria*. John Murray.
- Macdonald, G, Macdonald G (1957). *The Epidemiology and Control of Malaria*. Oxford University Press.
- MacKay, David JC (1992). “Bayesian interpolation”. In: *Neural Computation* 4.3, pp. 415–447.
- Gelman, Andrew, John B Carlin, et al. (1995). *Bayesian Data Analysis*. Chapman and Hall/CRC.
- Daley, Daryl J and Joe Gani (2001). *Epidemic Modelling: an Introduction*. 15. Cambridge University Press.
- Dunson, David B (2001). “Commentary: practical advantages of Bayesian analysis of epidemiologic data”. In: *American Journal of Epidemiology* 153.12, pp. 1222–1226.
- Ionides, Edward L, Carles Bretó, and Aaron A King (2006). “Inference for nonlinear dynamical systems”. In: *Proceedings of the National Academy of Sciences* 103.49, pp. 18438–18443.

- Bretó, Carles et al. (2009). “Time series analysis via mechanistic models”. In: *The Annals of Applied Statistics*, pp. 319–348.
- Beaumont, Mark A (2010). “Approximate Bayesian computation in evolution and ecology”. In: *Annual Review of Ecology, Evolution, and Systematics* 41.1, pp. 379–406.
- Blum, Michael GB and Olivier François (2010). “Non-linear regression models for approximate Bayesian computation”. In: *Statistics and Computing* 20, pp. 63–73.
- Britton, Tom (2010). “Stochastic epidemic models: a survey”. In: *Mathematical Biosciences* 225.1, pp. 24–35.
- He, Daihai, Edward L Ionides, and Aaron A King (2010). “Plug-and-play inference for disease dynamics: measles in large and small populations as a case study”. In: *Journal of the Royal Society Interface* 7.43, pp. 271–283.
- Toni, Tina and Michael PH Stumpf (2010). “Simulation-based model selection for dynamical systems in systems and population biology”. In: *Bioinformatics* 26.1, pp. 104–110.
- Wood, Simon N. (Aug. 2010). “Statistical inference for noisy nonlinear ecological dynamic systems”. In: *Nature* 466.7310, pp. 1102–1104. ISSN: 1476-4687.
- Cauchemez, Simon and Neil M. Ferguson (Aug. 2011). “Methods to infer transmission risk factors in complex outbreak data”. In: *Journal of The Royal Society Interface* 9.68, pp. 456–469. ISSN: 1742-5662.
- Ionides, Edward L. et al. (June 2011). “Iterated filtering”. In: *The Annals of Statistics* 39.3. ISSN: 0090-5364.
- Robert, Christian P et al. (2011). “Lack of confidence in approximate Bayesian computation model choice”. In: *Proceedings of the National Academy of Sciences* 108.37, pp. 15112–15117.
- Hilborn, Ray and Marc Mangel (2013). *The ecological detective: confronting models with data (MPB-28)*. Princeton University Press.
- Doan, Tan N. et al. (Dec. 2014). “Optimizing hospital infection control: the role of mathematical modeling”. In: *Infection Control & Hospital Epidemiology* 35.12, pp. 1521–1530. ISSN: 1559-6834.
- Papamakarios, George and Iain Murray (2016). “Fast  $\varepsilon$ -free inference of simulation models with Bayesian conditional density estimation”. In: *Advances in Neural Information Processing Systems* 29.
- Loshchilov, Ilya, Frank Hutter, et al. (2017). “Fixing weight decay regularization in adam”. In: *arXiv preprint arXiv:1711.05101* 5.
- Lueckmann, Jan-Matthis, Pedro J Goncalves, et al. (2017). “Flexible statistical inference for mechanistic models of neural dynamics”. In: *Advances in Neural Information Processing Systems* 30.
- McKinley, Trevelyan J. et al. (Feb. 2018). “Approximate Bayesian Computation and Simulation-Based Inference for Complex Stochastic Epidemic Models”. In: *Statistical Science* 33.1. ISSN: 0883-4237.
- Sisson, Scott A, Yanan Fan, and Mark Beaumont (2018). *Handbook of approximate Bayesian computation*. CRC Press.
- Ambrogioni, Luca et al. (2019). “Forward amortized inference for likelihood-free variational marginalization”. In: *The 22nd International Conference on Artificial Intelligence and Statistics*. PMLR, pp. 777–786.
- Baydin, Atilim Gunes et al. (2019). “Efficient probabilistic inference in the quest for physics beyond the standard model”. In: *Advances in Neural Information Processing Systems* 32.
- Minter, Amanda and Renata Retkute (Dec. 2019). “Approximate Bayesian Computation for infectious disease modelling”. In: *Epidemics* 29, p. 100368. ISSN: 1755-4365.
- Papamakarios, George (2019). “Neural density estimation and likelihood-free inference”. In: *arXiv preprint arXiv:1910.13233*.
- Cranmer, Kyle, Johann Brehmer, and Gilles Louppe (2020). “The frontier of simulation-based inference”. In: *Proceedings of the National Academy of Sciences* 117.48, pp. 30055–30062.
- Gelman, Andrew, Aki Vehtari, et al. (2020). “Bayesian workflow”. In: *arXiv preprint arXiv:2011.01808*.
- Dax, Maximilian et al. (2021). “Real-time gravitational wave science with neural posterior estimation”. In: *Physical Review Letters* 127.24, p. 241103.
- Lueckmann, Jan-Matthis, Jan Boelts, et al. (2021). “Benchmarking simulation-based inference”. In: *International Conference on Artificial Intelligence and Statistics*. PMLR, pp. 343–351.
- Papamakarios, George, Eric Nalisnick, et al. (2021). “Normalizing flows for probabilistic modeling and inference”. In: *Journal of Machine Learning Research* 22.57, pp. 1–64.
- Radev, Stefan T et al. (2021). “OutbreakFlow: Model-based Bayesian inference of disease outbreak dynamics with invertible neural networks and its application to the COVID-19 pandemics in Germany”. In: *PLoS Computational Biology* 17.10, e1009472.
- Bu, Fan et al. (2022). “Likelihood-based inference for partially observed epidemics on dynamic networks”. In: *Journal of the American Statistical Association* 117.537, pp. 510–526.
- Fintzi, Jonathan, Jon Wakefield, and Vladimir N Minin (2022). “A linear noise approximation for stochastic epidemic models fit to partially observed incidence counts”. In: *Biometrics* 78.4, pp. 1530–1541.
- Hawken, Shawn E et al. (2022). “Threshold-free genomic cluster detection to track transmission pathways in health-care settings: a genomic epidemiology analysis”. In: *The Lancet Microbe* 3.9, e652–e662.
- Zelner, Jon and Marisa Eisenberg (2022). “Rapid response modeling of SARS-CoV-2 transmission”. In: *Science* 376.6593, pp. 579–580.

- Karampatakis, Theodoros, Katerina Tsergouli, and Payam Behzadi (2023). “Carbapenem-resistant *Klebsiella pneumoniae*: virulence factors, molecular epidemiology and latest updates in treatment options”. In: *Antibiotics* 12.2, p. 234.
- Liu, Runjing et al. (2023). “Variational inference for deblending crowded starfields”. In: *Journal of Machine Learning Research* 24.179, pp. 1–36.
- Simons, Jack et al. (2023). “Neural score estimation: Likelihood-free inference with conditional score based diffusion models”. In: *Fifth Symposium on Advances in Approximate Bayesian Inference*.
- Spurio Mancini, A et al. (2023). “Bayesian model comparison for simulation-based inference”. In: *RAS Techniques and Instruments* 2.1, pp. 710–722.
- Vasist, Malavika et al. (2023). “Neural posterior estimation for exoplanetary atmospheric retrieval”. In: *Astronomy & Astrophysics* 672, A147.
- Healthcare Research, Agency for and Quality (2024). *Health Care-Associated Infections*. URL: <https://www.ahrq.gov/professionals/quality-patient-safety/patient-safety-resources/resources/hais/index.html> (visited on 01/03/2024).
- King, Aaron (2024). *Simulation of Stochastic Dynamic Models*. URL: <https://kingaa.github.io/clim-dis/> (visited on 05/12/2024).

## A SI Model

### B Monte Carlo Posterior Estimation

#### B.1 Likelihood-based Inference

A simple, likelihood-based estimator of the posterior can be found using Rejection Sampling. Let  $M = \max_{\theta \in \Theta} p(\mathbf{x}_o | \theta)$ . (This is the likelihood density evaluated at the MLE.) Let  $S$  be our target sample size. For  $s = 1, \dots, S$ :

1. Draw  $\theta' \sim p(\theta)$ .
2. Draw  $u \sim \text{Unif}(0, 1)$ .
3. Compute acceptance probability

$$A = \frac{p(\theta, \mathbf{x}_o)}{Mp(\theta)} = \frac{p(\mathbf{x}_o | \theta)}{M}$$

4. If  $u < A$ , then set  $\theta^{(s)} = \theta'$ . Otherwise go back to step 1.

In words, we sample many parameters from the prior and are more likely to accept them into our estimated posterior sample if their likelihood is high. This naive algorithm can be quite inefficient if the prior is not concentrated around the MLE, but it gives an unbiased estimate of the posterior<sup>19</sup> with minimal engineering and design (e.g. as compared to MCMC).

#### B.2 Likelihood-free Inference

The basic Approximate Bayesian Computation (ABC) algorithm is analogous to Rejection Sampling. As before, let  $S$  denote the desired sample size of the posterior estimate. Fix  $\epsilon > 0$  to be the error threshold and let  $\|\cdot\|$  be a distance metric (e.g. Euclidean distance). Let  $g(\cdot)$  define a summary statistic for  $\mathbf{x}$ .

For  $s = 1, \dots, S$ :

1. Draw  $\theta' \sim p(\theta)$ .
2. Simulate  $\mathbf{x}' \sim p(\mathbf{x} | \theta')$ .
3. If  $\|g(\mathbf{x}') - g(\mathbf{x}_o)\| < \epsilon$ , then set  $\theta^{(s)} = \theta'$ . Otherwise, go back to step 1.

#### B.3 Data Likelihood

We derive the likelihood written out in equations 13, 14, and 15 from the following individual transition probabilities. For  $1 \leq t \leq T$ ,

<sup>19</sup><https://stats.stackexchange.com/questions/407112/proving-the-accepted-samples-from-rejection-sampling-follows->

- $P(X_t^{(i)} = 0 \mid X_{t-1}^{(i)} = 0) = \gamma(1 - \alpha) + (1 - \gamma)(e^{-\lambda_i(t)})$ 
  - A susceptible patient is discharged and replaced with a susceptible or is not discharged and fails to get infected
- $P(X_t^{(i)} = 0 \mid X_{t-1}^{(i)} = 1) = \gamma(1 - \alpha)$ 
  - An infected patient is discharged and replaced with a susceptible
- $P(X_t^{(i)} = 1 \mid X_{t-1}^{(i)} = 0) = \gamma\alpha + (1 - \gamma)(1 - e^{-\lambda_i(t)})$ 
  - A susceptible patient is discharged and replaced with an infected or is not discharged and gets infected
- $P(X_t^{(i)} = 1 \mid X_{t-1}^{(i)} = 1) = \gamma\alpha + (1 - \gamma)$ 
  - An infected patient is discharged and replaced with an infected or is not discharged

The asymmetry in transition probabilities between already-infected and already-susceptible patients arises from the assumption that an infected patient stays infected without recovery. It follows that the transition likelihood for an individual patient is

$$P(X_t^{(i)} \mid X_{t-1}^{(i)}) = \left[ \gamma\alpha + (1 - \gamma)(1 - e^{-\lambda_i(t)})^{(1 - X_{t-1}^{(i)})} \right]^{X_t^{(i)}} \cdot \left[ \gamma(1 - \alpha) + (1 - \gamma)(e^{-\lambda_i(t)})^{(1 - X_{t-1}^{(i)})} \right]^{(1 - X_t^{(i)})}. \quad (20)$$

## C Summary Statistics

To estimate the vector of heterogeneous infection rates  $\beta$ , we process the raw infection status data  $\mathbf{X}$  into seven location-specific summary statistics or “views,” which we write as  $\mathbf{J}$ . We can think of  $\mathbf{J}$  as a  $T \times (K + 2)$  matrix, where  $K$  is the number of floors. Written in column form,

$$\mathbf{J} = (\mathbf{I} \quad \mathbf{L}_1 \quad \dots \quad \mathbf{L}_K \quad \mathbf{R}), \quad (21)$$

where

- $\mathbf{I} = \{I_1, \dots, I_T\}$  is the overall case count over time. (Recall that  $I_t = \sum_{i=1}^N X_t^{(i)}$ . This is the same summary statistic used for estimating the homogeneous infection rate.
- For every  $k = 1, \dots, K$  and  $t = 1, \dots, T$ , define

$$L_{k,t} = \sum_{i:F(i)=k} X_t^{(i)}, \quad (22)$$

with  $F(i)$  indicating the floor on which patient  $i$  resides. Then,  $\mathbf{L}_k = \{L_{k,1}, \dots, L_{k,T}\}$ . This is the number of cases over time on each floor.

- For each  $t = 1, \dots, T$  and  $i = 1, \dots, N$ , we define  $Q_t^{(i)}$ , to be the number of infected patients at time  $t$  in the room belonging to patient  $i$ . Suppose there are  $N_R$  rooms. We define

$$R_t = \#\{i : Q_t^{(i)} > 1\} \quad (23)$$

Then,  $\mathbf{R} = \{R_1, \dots, R_T\}$ . We can think of this statistic as measuring the number of rooms with multiple infected patients, which should intuitively correlate with the risk of roommate-roommate transmission.

It is greatly beneficial for deep learning models to standardize input data such that variance is comparable across multiple features. To this end, we rescale all statistics so that they fall between 0 and 1. We divide  $I$  by  $N$ , the overall patient population. When the facility population variable, as in the CRKP dataset, we divide by the maximum observed population over the period of study.) Likewise, we divide  $\mathbf{L}_1, \dots, \mathbf{L}_K$  by the population (or maximum capacity) of each floor, and divide  $\mathbf{R}$  by the number of unique rooms.

## D Partial Observation Likelihood

We assume the simplest case where  $\gamma = 0$ , that is, no random turnover of patients.

$$P(Y_1^{(i)} \mid X_1^{(i)}) = \begin{cases} (1 - \eta)^{X_1^{(i)}} & \text{if } Y_1^{(i)} = 0 \\ 1 - (1 - \eta)^{X_1^{(i)}} & \text{if } Y_1^{(i)} = 1 \end{cases}$$

Table 5: 90% credible intervals (corresponding to the (0.05, 0.95) quantiles) for heterogeneous infection rates.

Transmission Rate	Value	90% CI		
		Exact	NPE	ABC
Facility	0.05	(0.0240, 0.0680)	(0.0250, 0.0785)	(0.0210, 0.0943)
Floor 1	0.02	(0.00493, 0.0424)	(-0.00600, 0.0684)	(0.00639, 0.0692)
Floor 2	0.04	(0.0327, 0.0928)	(0.00530, 0.0843)	(0.0118, 0.119)
Floor 3	0.06	(0.0165, 0.0732)	(0.0113, 0.0892)	(0.0117, 0.0773)
Floor 4	0.08	(0.0285, 0.0982)	(0.0215, 0.111)	(0.0142, 0.116)
Floor 5	0.1	(0.0709, 0.148)	(0.0527, 0.143)	(0.0183, 0.152)
Room	0.05	(0.0284, 0.0621)	(0.00279, 0.0800)	(0.00979, 0.152)

and for  $t > 1$ ,

$$P(Y_t^{(i)} | Y_{t-1}^{(i)}, X_1^{(i)}, \dots, X_t^{(i)}) = \begin{cases} (1 - \eta)^{W_t^{(i)}} & \text{if } Y_t^{(i)} = 0 \wedge Y_{t-1}^{(i)} = 0 \\ 0 & \text{if } Y_t^{(i)} = 0 \wedge Y_{t-1}^{(i)} = 1 \\ 1 - (1 - \eta)^{W_t^{(i)}} & \text{if } Y_t^{(i)} = 1 \wedge Y_{t-1}^{(i)} = 0 \\ 1 & \text{if } Y_t^{(i)} = 1 \wedge Y_{t-1}^{(i)} = 1 \end{cases},$$

where  $W_t^{(i)} = \sum_{s=1}^t X_s^{(i)}$ . Let  $S_i = \min\{t : Y_t^{(i)} = 1\}$  (or  $T + 1$  if this is undefined). Let  $\tilde{S}_i = \min\{t : X_t^{(i)} = 1\}$  (or  $T + 1$  if this is undefined).

$$P(Y_t^{(i)} = 1 | X_1^{(i)}, \dots, X_t^{(i)}) = P(S_i \leq t | X_1^{(i)}, \dots, X_t^{(i)}),$$

and  $S_i - \tilde{S}_i$  follows a geometric distribution. Thus,

$$\begin{aligned} P(S_i \leq t | X_1^{(i)}, \dots, X_t^{(i)}) &= P(S_i - \tilde{S}_i \leq t - \tilde{S}_i | X_1^{(i)}, \dots, X_t^{(i)}) \\ &= 1 - (1 - \eta)^{t - \tilde{S}_i + 1} = 1 - (1 - \eta)^{W_t^{(i)}}. \end{aligned}$$

Therefore we can compute

$$P(Y_i | X_i) = P(Y_1^{(i)} | X_1^{(i)}) \prod_{t=2}^T P(Y_t^{(i)} | Y_{t-1}^{(i)}, X_1^{(i)}, \dots, X_t^{(i)})$$

and

$$P(\mathbf{Y} | \mathbf{X}) = \prod_{i=1}^N P(Y_i | X_i).$$

## E Supplemental Figures and Tables

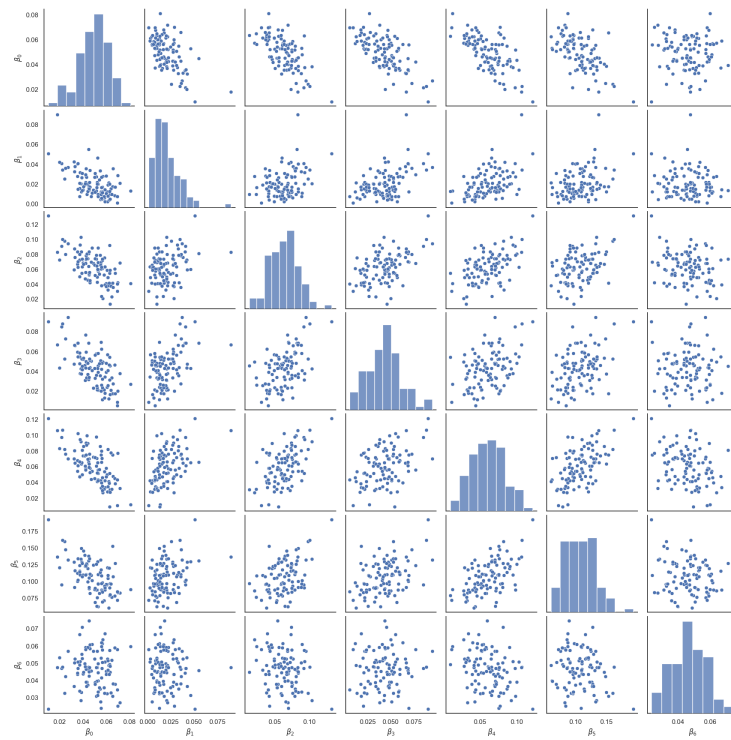
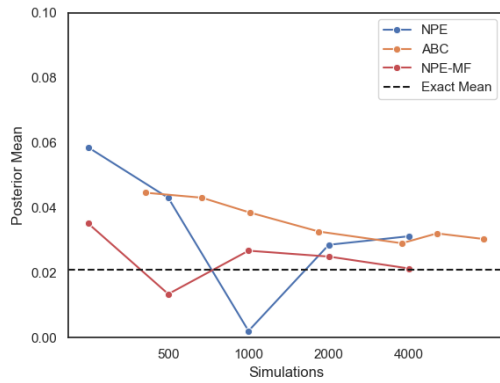
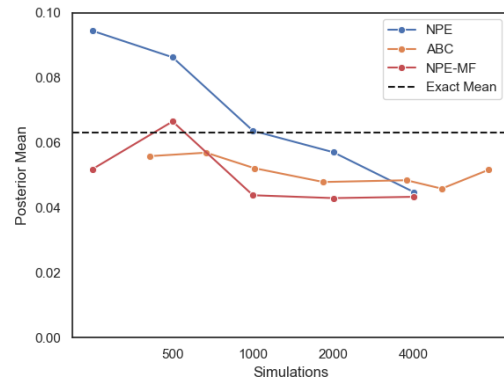


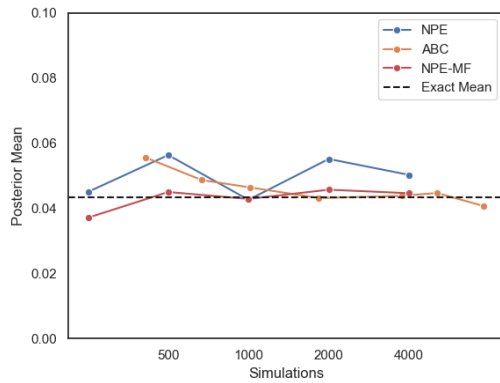
Figure 15: Pair plot of the exact, likelihood-based sample of heterogeneous infection rates on the natural scale. Note the elliptical, approximately Gaussian covariance structure.



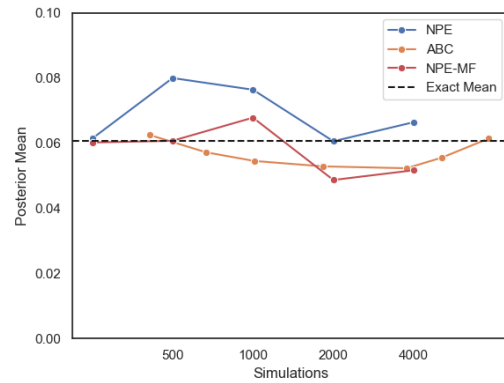
(a) Estimation of the infection rate within Floor 1,  $\beta_1$ .



(b) Estimation of the infection rate within Floor 2,  $\beta_2$ .

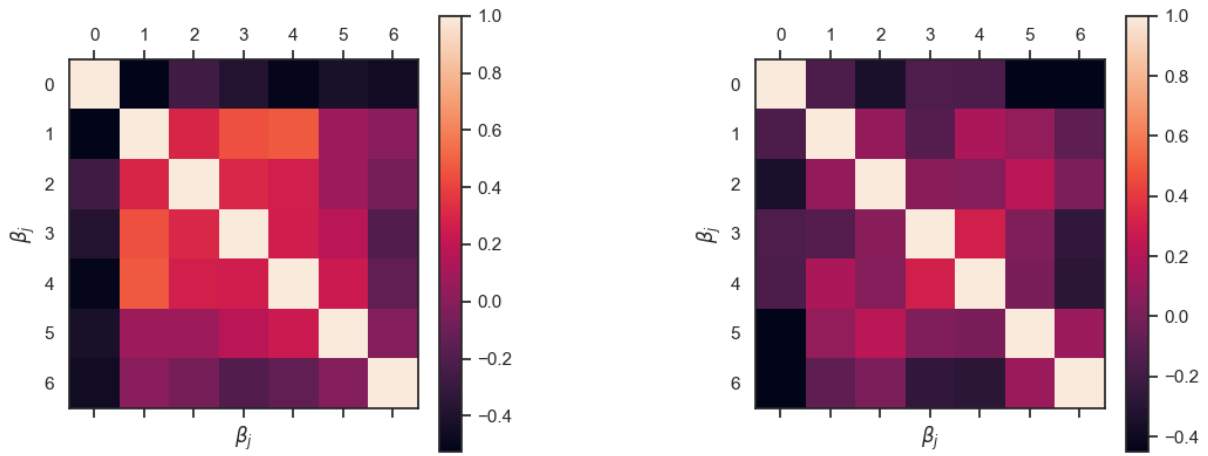


(c) Estimation of the infection rate within Floor 3,  $\beta_3$ .



(d) Estimation of the infection rate within Floor 4,  $\beta_4$ .

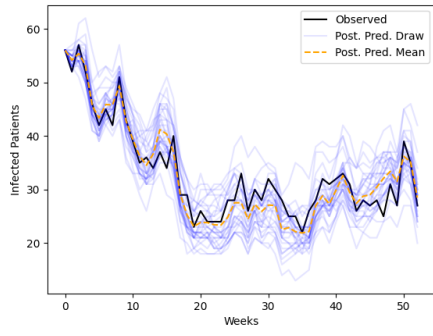
Figure 16: Simulation-based estimation accuracy and sample-efficiency for heterogeneous infection rates (simulated experiment).



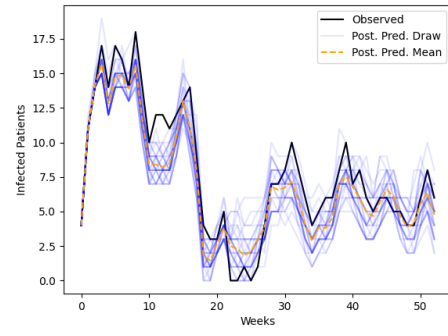
(a) NPE posterior correlations (truncated MVN approximation)

(b) ABC posterior correlations

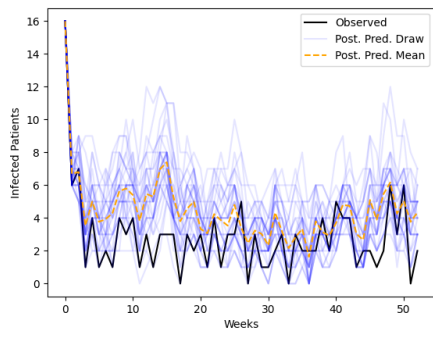
Figure 17: Correlation heatmaps for the simulation-based approximate posterior distribution of heterogeneous infection rates  $\beta$  under partial observation of cases.



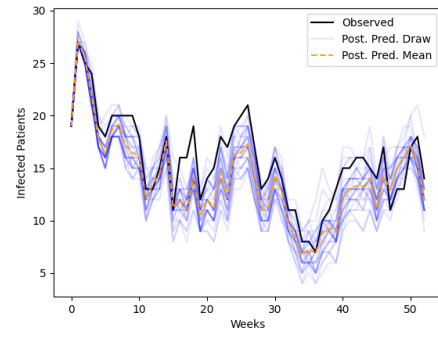
(a) Facility



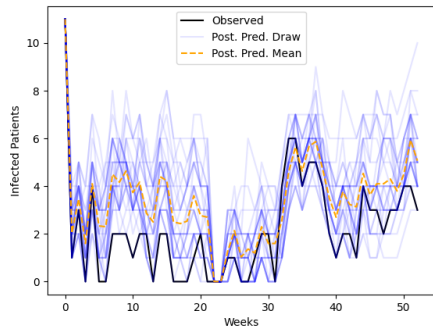
(b) Floor 1



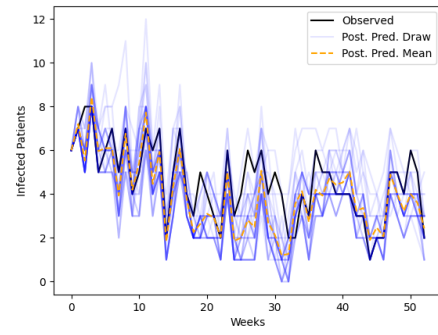
(c) Floor 2



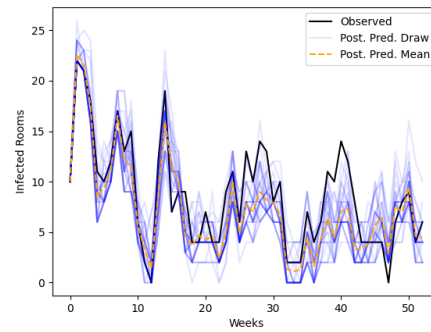
(d) Floor 3



(e) Floor 4



(f) SCU (Floor 5)



(g) Room

Figure 18: Posterior predictive checks of the NPE-estimated homogeneous infection rate for the CRKP dataset.

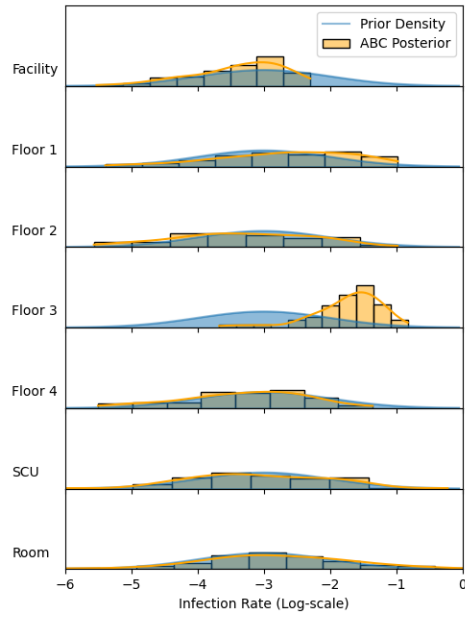
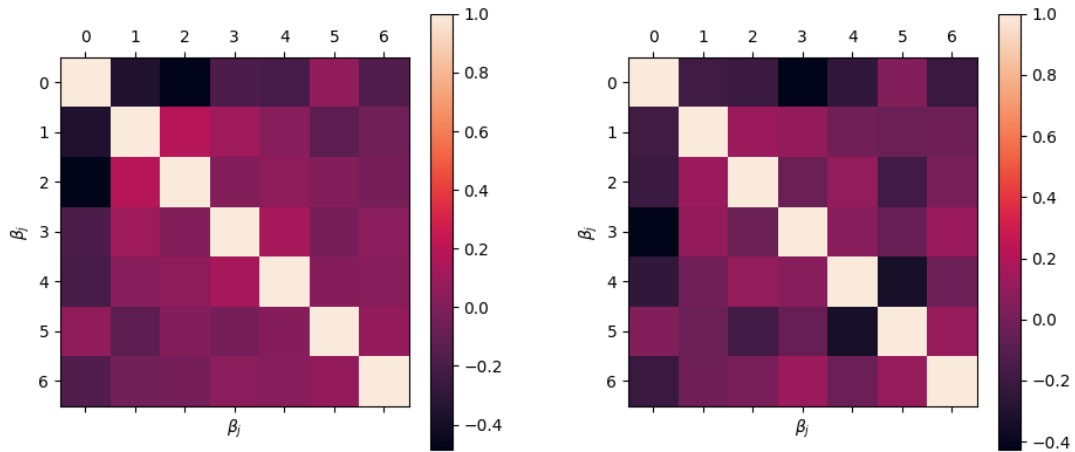


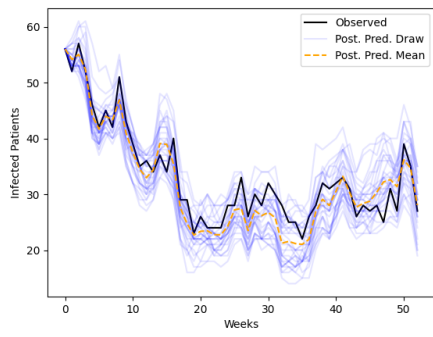
Figure 19: Comparison of the ABC approximate posterior heterogeneous infection rates and the prior.



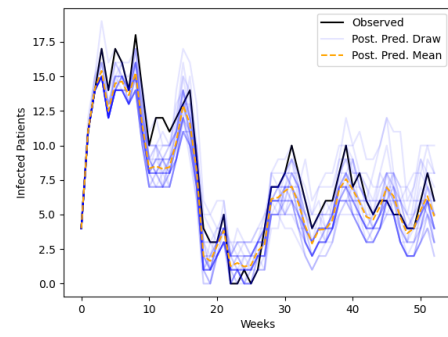
(a) NPE correlation matrix

(b) ABC correlation matrix

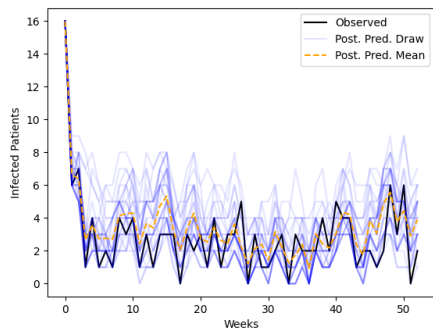
Figure 20: Correlation matrices for heterogeneous CRKP infection rates.



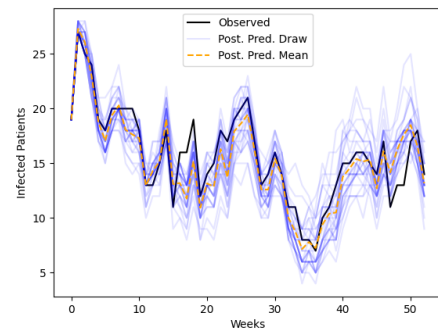
(a) Facility



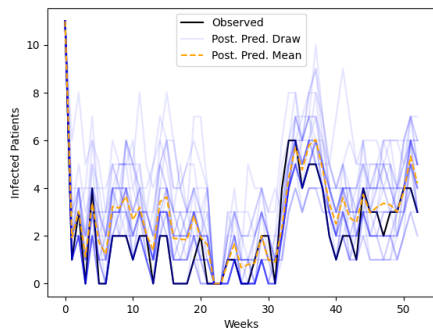
(b) Floor 1



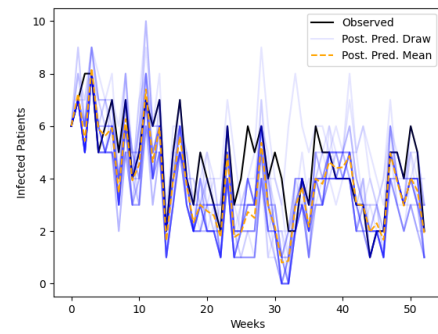
(c) Floor 2



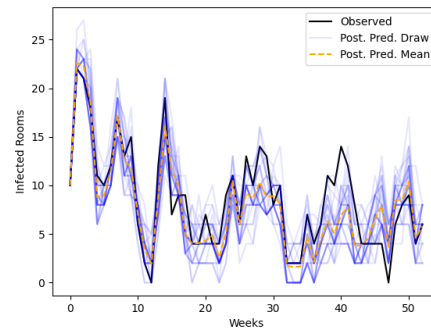
(d) Floor 3



(e) Floor 4



(f) SCU (Floor 5)



(g) Room

Figure 21: Posterior predictive checks of the ABC-estimated heterogeneous infection rates for the CRKP dataset.

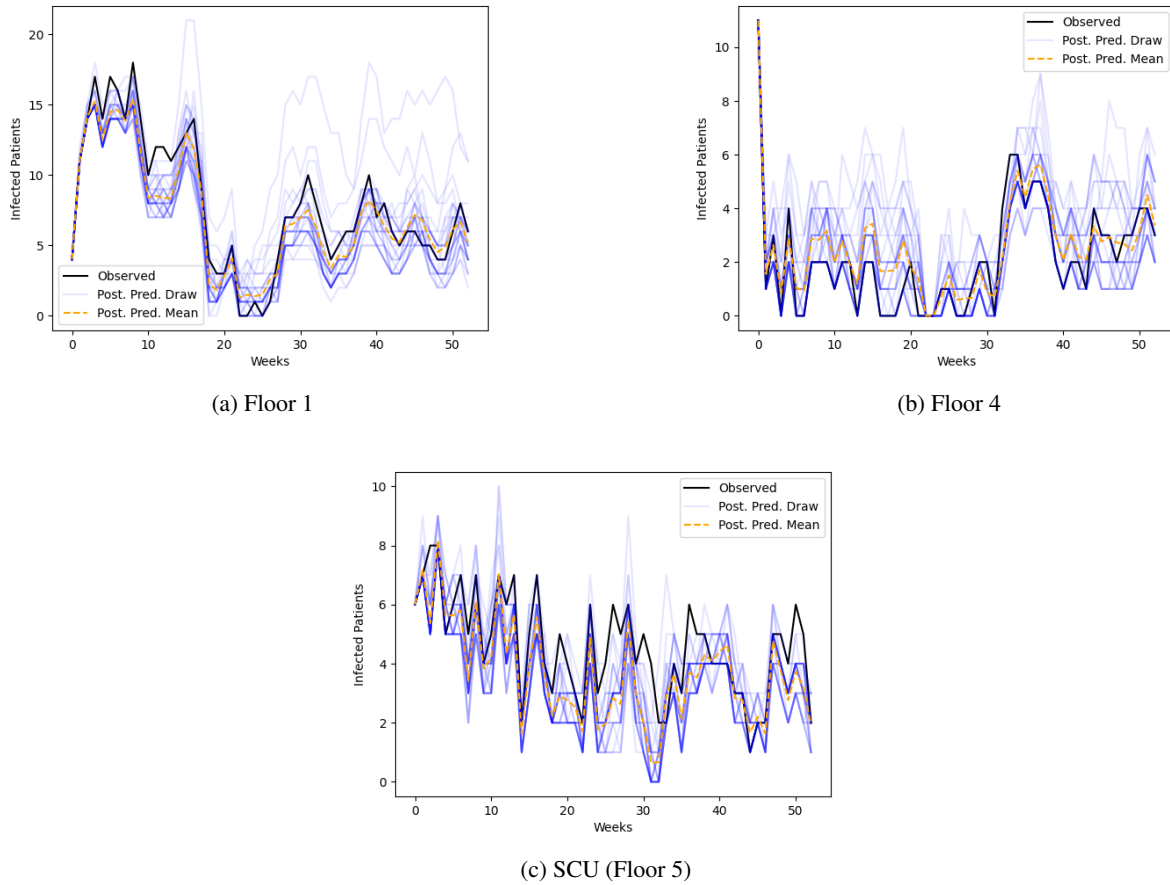


Figure 22: Posterior predictive checks of the NPE-estimated heterogeneous infection rates for the CRKP dataset.